The EMBO Journal Vol. 22 No. 7 pp. 1539–1554, 2003

Regulation of cell–cell interactions by phosphatidic acid phosphatase 2b/VCIP

Joseph O.Humtsoe, Shu Feng, Geeta D.Thakker[1], Jun Yang, Jun Hong and Kishore K.Wary[2]

Center for Extracellular Matrix Biology, Institute of Biosciences and Technology, Texas Medical Center, 2121 W. Holcombe Blvd, Houston, TX 77030, USA

[1]Present address: Lexicon Genetics Inc., 8800 Technology Forest Drive, The Woodlands, TX 77831, USA

[2]Corresponding author
e-mail: kwary@ibt.tamu.edu

J.O.Humtsoe and S.Feng contributed equally to this work

We identified vascular endothelial growth factor and type I collagen inducible protein (VCIP), also known as phosphatidic acid phosphatase 2b (PAP2b), in a functional assay of angiogenesis. VCIP/PAP2b exhibits an Arg–Gly–Asp (RGD) cell adhesion sequence. Immunoprecipitation and fluorescence-activated cell sorting analyses demonstrated that VCIP-RGD is exposed to the outside of the cell surface. Retroviral transduction of VCIP induced cell aggregation/cell–cell interactions, modestly increased p120 catenin expression and promoted activation of the Fak, Akt and GSK3β protein kinases. Furthermore, expression of recombinant VCIP promoted adhesion, spreading and tyrosine phosphorylation of Fak, Shc, Cas and paxillin in endothelial cells. GST–VCIP-RGD, but not GST–VCIP-RGE, specifically interacted with a subset of integrins, and these interactions were effectively blocked by anti-$\alpha_v\beta_3$ and anti-$\alpha_5\beta_1$ integrin antibodies, and by PAP2b/VCIP-derived peptides. Interestingly, PAP2b/VCIP is expressed in close proximity to vascular endothelial growth factor, von Willebrand factor and $\alpha_v\beta_3$ integrin in tumor vasculatures. These findings demonstrate an unexpected function of PAP2b/VCIP, and represent an important step towards understanding the molecular mechanisms by which PAP2b/VCIP-induced cell–cell interactions regulate specific intracellular signaling pathways.
Keywords: cell–cell interactions/endothelial cells/integrins/signaling/VEGF

Introduction

Cell–cell and cell–matrix interactions play fundamental roles in embryonic development and in wound healing, and these interactions are known to be altered in many pathological processes. Endothelial cells (ECs), which line the walls of blood vessels, are able to promote both 'homotypic' and 'heterotypic' cell–cell interactions (Cines *et al*., 1998). Such interactions are critical for angiogenesis, which proceeds through several distinct coordinated steps. Initially, ECs that are contact inhibited or considered to be in the G_0 phase of the cell cycle become activated in response to an increase in local concentrations of angiogenic factors (Cotta-Pereira *et al*., 1980). Activated ECs then locally secrete proteases to dissolve basement membranes, thereby allowing ECs to detach from the vascular wall. The detached ECs then send out cytoplasmic projections, migrate, elongate extensively and form cell–cell interactions (Montesano *et al*., 1985). Eventually, ECs enter the cell cycle and can either differentiate into tube-like structures, depending upon the presence of specific survival factors and extracellular matrix (ECM) components, or undergo apoptosis, which can disrupt angiogenesis (Risau and Flamme, 1995). These *in vivo* processes can be partially duplicated *in vitro* by providing ECs with appropriate ECM molecules and a gradient of angiogenic cytokines, such as basic fibroblast growth factor (bFGF) and vascular endothelial growth factor (VEGF) (Pepper *et al*., 1992; Friesel and Maciag, 1995; Dvorak, 2000). VEGF and bFGF can act on ECs either individually or in a coordinated manner to transduce extracellular signals into distinct cellular transcriptional responses (Yancopoulos *et al*., 2000; Cross and Claesson-Welsh, 2001). The specific roles of VEGF and its receptors in angiogenesis have been well documented. For example, genetic ablation of the VEGF receptor-2 (Flk-1) in mice causes loss of functional ECs (Shalaby *et al*., 1995). Ablation of the $VEGF^{165}$ gene, which encodes the Flk-1 ligand, results in a complete lack of vasculature, and this genotype is embryonic lethal (Carmeliet *et al*., 1996). Angiopoietin (Ang) and Ephrins signal through Tie and Eph receptors, respectively (Suri *et al*., 1996; Yancopoulos *et al*., 1998). The intracellular Ang signaling pathway determines the maturity of blood vessels, whereas Eph regulates segregation of arteries and veins (Wang *et al*., 1998). While most of these factors directly regulate normal angiogenesis, unrestrained production of these factors can potentially deregulate cell–cell interactions, cell–matrix interactions and gene expression. Such deregulation may contribute to various vascular abnormalities, including the growth of solid tumors, cardiovascular disease and diabetic retinopathy (Folkman, 2001).

Activated ECs detach from the endothelium and maintain cell–cell contact in order to survive; the absence of such cell–cell interactions can promote anoikis (Frisch and Ruoshlati, 1997). Studies suggest that EC-mediated cell–cell interactions are also required for the recruitment of pericytes, as well as for the stabilization and maturation of blood vessels (Darland and D'Amore, 2001). Molecules that mediate cell–cell interactions include integrins and their ligands, VE-cadherin, PECAM-1 (CD31), junctional adhesion molecules (JAM), VCAM-1, selectins, claudins, Eph and Ephrins (Lampugnani and Dejana, 1997; Eliceiri and Cheresh, 2001). These adhesion molecules are also

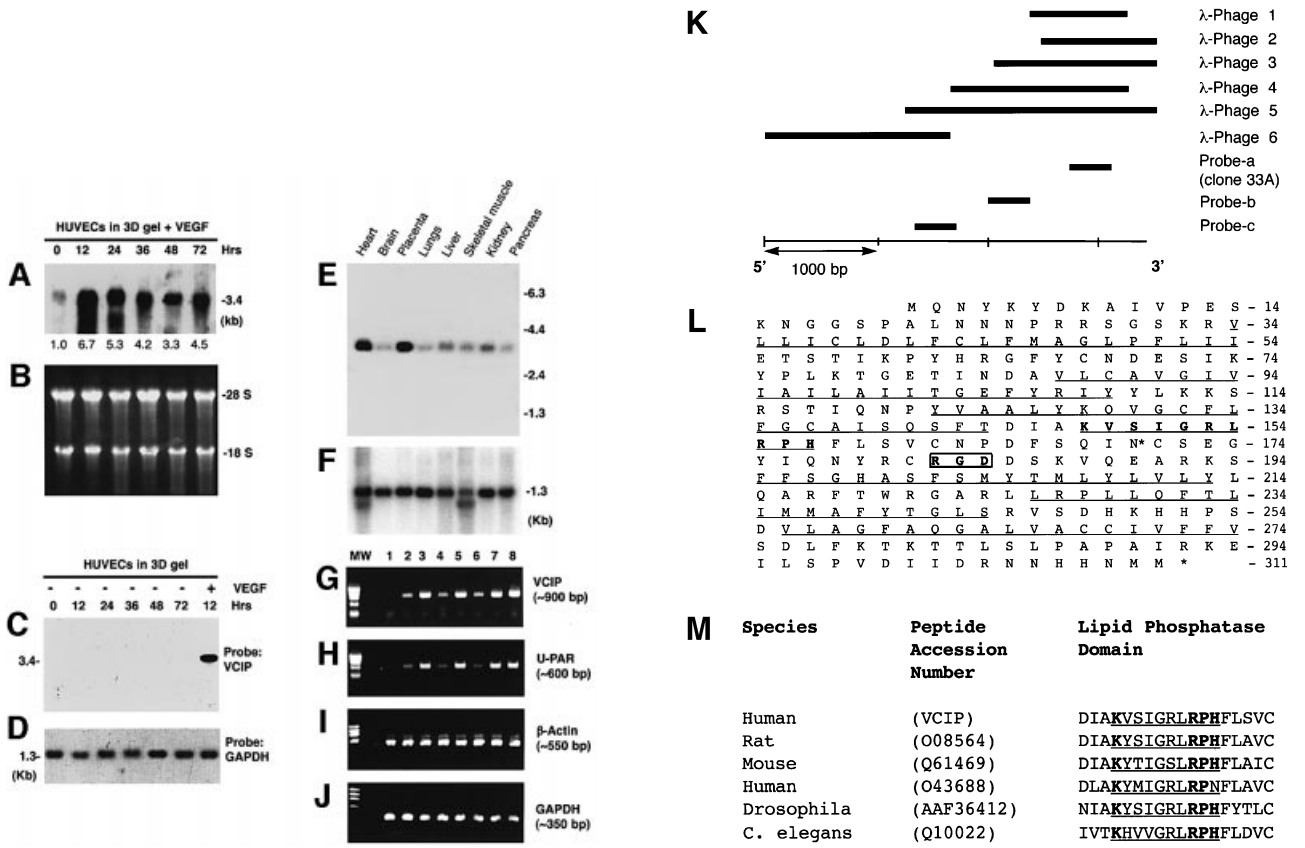

Fig. 1. Expression analysis and predicted amino acid sequence of VCIP. HUVECs were embedded into three-dimensional type I collagen gel in the presence of 20% adult human serum, 1× ITS and stimulated with VEGF^{165} (100 ng/ml). Total RNA was prepared at the indicated time points. (**A**) Northern blots were hybridized with a fragment of the VCIP (clone-33A) cDNA probe. The transcript size (3.4 kb) is indicated on the right. The numbers at the bottom of the gel represent the fold increase in VCIP mRNA levels, as compared with untreated cells. (**B**) Ethidium bromide-stained agarose gel shows equivalent amounts of RNA used. (**C**) HUVECs were cultured as above and left untreated, the last lane shows cells treated with VEGF for 12 h, as a positive control. Total RNA was isolated at indicated time points and subjected to VCIP northern blot analysis. (**D**) The blot shown in (C) was stripped and re-hybridized with a GAPDH probe, to show that equal amounts of RNA were loaded across the lanes. (**E**) Poly(A)$^+$ RNA prepared from various human tissues was subjected to VCIP northern blot analysis by hybridization with the clone-33A cDNA probe. (**F**) The blot shown in (C) was re-hybridized with a GAPDH probe, showing that equal amounts of RNA were loaded across the lanes. (**G**) Detection of VCIP mRNA by RT–PCR (20 cycles): monolayer ECs were treated for 30 min with: (1) untreated, (2) + bFGF (20 ng/ml), (3) + VEGF^{165} (100 ng/ml), (4) + PMA (20 ng/ml), (5) + bFGF (20 ng/ml) + VEGF (100 ng/ml), (6) bFGF (20 ng/ml) + PMA (20 ng/ml), (7) VEGF (100 ng/ml) + PMA (20 ng/ml) and (8) bFGF (20 ng/ml) + VEGF (100 ng/ml) + PMA (20 ng/ml). (**H–J**) RT–PCR analysis of (H) uPAR mRNA, (I) β-actin mRNA and (J) GAPDH mRNA levels under the same conditions as described in (G). All experiments were repeated at least three times, with similar results. (**K**) Inserts from six recombinant λ phage clones are shown, and the relative position of clone 33A is indicated. (**L**) The complete predicted amino acid sequence of VCIP. The putative transmembrane segments are underlined. The *N*-linked glycosylation site is indicated by an asterisk. The lipid phosphatase catalytic domain is indicated by bold letters and underlined, and the RGD motif is boxed. (**M**) The amino acid sequence of human VCIP (top) is aligned with other proteins containing lipid phosphatase-like catalytic motifs.

involved in the assembly and formation of adherent and tight junctions, phenotypes that are closely associated with the formation of mature blood vessels and the segregation of arteries and veins (Dejana, 1997; Hirschi and D'Amore, 1997). Although a large number of studies have investigated the formation of cell–cell contacts, the molecular mechanisms underlying this process are not completely understood (Darland and D'Amore, 2001).

The addition of angiogenic factors to quiescent ECs, cultured in three-dimensional type I collagen matrices, induces capillary morphogenesis (Madri and Williams, 1983; Montesano and Orci, 1985). To better understand the molecular pathways that control the formation of new blood vessels, we recently identified a set of 12 novel genes, derived from ECs undergoing capillary morphogenesis in three-dimensional collagen matrices (K.K.Wary, G.D.Thakker, J.O.Humtsoe, S.Feng and J.Yang, submitted for publication). These 12 genes had not been previously reported to be associated with the processes of angiogenesis. We have now characterized the function of one of these genes (DDBJ/EMBL/GenBank accession No. AF480883), designated VCIP for VEGF and type I collagen inducible protein, which is also known as phosphatidic acid phosphatase type 2b (PAP2b) (Kai *et al*., 1997). Interestingly, PAP2b also contains an Arg–Gly–Asp (RGD) cell attachment sequence. The RGD motif, present in many known ECM proteins, is an established core recognition sequence for the $\alpha_5\beta_1$, $\alpha_v\beta_3$, $\alpha_v\beta_5$, $\alpha_v\beta_1$ and $\alpha II_b\beta_3$ integrins (Hynes, 1987; Ruoslahti and Pierschbacher, 1987). Many laboratories have investigated the physiological roles of ECM proteins containing the RGD cell attachment motif (Varner and Cheresh, 1996; Plow *et al*., 2000; Humphries, 2002). Binding of integrins to RGD-containing ligands promotes adhesion,

spreading and 'outside-in' signaling. These signals regulate tyrosine phosphorylation of various intracellular proteins, calcium influx, changes in pH and gene expression (Giancotti and Ruoslahti, 1999; Martin *et al*., 2002; Schwartz and Ginsberg, 2002).

In this study, we present several lines of compelling evidence that reveal a unique role for VCIP in cell–cell interactions and intracellular signaling. To our knowledge, this is the first report describing these novel functions of VCIP.

Results

Identification of PAP2b/VCIP

In a previous study, ECs were embedded into three-dimensional type I collagen gel and induced to undergo capillary morphogenesis in response to $VEGF^{165}$. RNA was then isolated from ECs cultured in the presence or absence of $VEGF^{165}$, converted to cDNA and subjected to suppression subtractive hybridization and differential display. Through this process, we identified a set of 12 candidate genes associated with capillary morphogenesis in ECs (K.K.Wary, G.D.Thakker, J.O.Humtsoe, S.Feng and J.Yang, submitted). One of the gene fragments (~500 bp) identified with this approach was of particular interest. Initial northern blot analyses suggested that its expression required presence of VEGF (Figure 1A and C). In a subsequent study, we found that the addition of anti-VEGF and or anti-$\alpha_2\beta_1$ integrin (type I collagen receptor) antibodies partially blocked expression of VCIP in ECs (Supplementary figure 1, available at *The EMBO Journal* Online). For this reason, we proposed the name VCIP. In addition, VCIP mRNA was most strongly expressed in human heart and placenta, tissues that are highly vascularized (Figure 1E). Next, we examined expression of VCIP in monolayer ECs treated with bFGF, VEGF and PMA (Figure 1G). We found that all three cytokines are equally able to induce expression of VCIP. This pattern of regulation was identical to that of the human receptor for urokinase plasminogen activator (uPAR) expression (Figure 1H); β-actin and GAPDH were included as controls and were not regulated under any of these conditions (Figure 1I and J). Nevertheless, these findings compelled us to clone the VCIP gene and investigate its possible role in capillary morphogenesis of ECs.

During our initial cloning effort, we sequenced several 3′ ends of RT–PCR products derived from a pool of 3′ and 5′ RACE products using DNA sequence information from clone 33A, as shown in Figure 1K. We sequenced ~2.0 kb of a 3′ region of a putative gene, which did not exhibit an open reading frame (ORF). Two 5′ probes were generated from this 2.0 kb fragment, and used to screen a human placental cDNA library, resulting in the recovery of six λ-phage cDNA clones (Figure 1K). Sequencing analysis revealed that one of the cDNA fragments of ~1.5 kb in size contained an ORF of 930 bp (λ-phage 6; Figure 1K), which clearly corresponded to the PAP2b gene (Kai *et al*., 1997). In fact, the cDNA that we designated as VCIP turned out to be identical to PAP2b, which encodes a 3.4 kb transcript. This is much larger than the transcript size that was previously reported for PAP2b (Kai *et al*., 1997). However, our data show that PAP2b/VCIP (henceforth called VCIP) has an unusually long 3′ untranslated region (UTR) of ~2.0 kb. The complete cDNA sequence of VCIP has been deposited under the accession No. AF480883, and the deduced amino acid sequence of VCIP is shown in Figure 1L. Database searches with the VCIP coding sequence and analysis of the deduced amino acid sequence revealed that VCIP has a consensus lipid phosphatase motif and an RGD cell attachment sequence in the second extracellular domain, whereas the cytoplasmic domains of VCIP lack any known enzymatic features or motifs. The lipid phosphatase motif of VCIP is shown in comparison with other known lipid phosphatase motifs in Figure 1M.

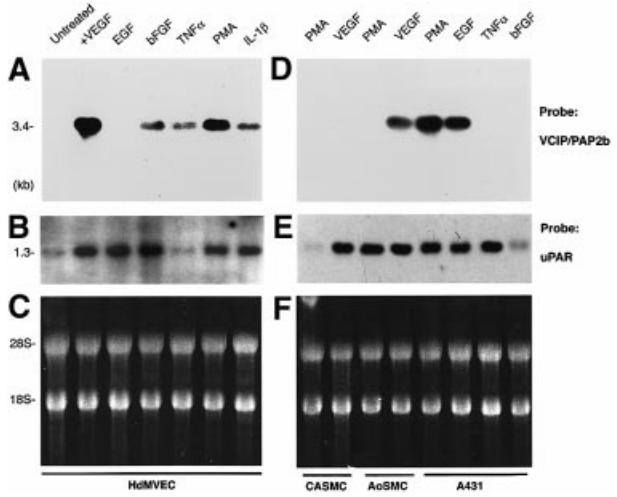

Fig. 2. Growth factors and cytokines induce expression of VCIP. (**A** and **D**) Indicated monolayer cells were stimulated with various growth factors and cytokines for 6 h in media M199 containing 10% serum + 1× ITS. The concentrations of cytokines used in this study were optimized according to their ability to induce Erk2 phosphorylation in western blot analysis: $VEGF^{165}$ (100 ng/ml), EGF (20 ng/ml), bFGF (30 ng/ml), TNFα (15 ng/ml), PMA (10 ng/ml) and IL-1β (25 ng/ml). Total RNA (20 μg per lane) was subjected to northern blot analysis by hybridization with the indicated probes. (**B** and **E**) The uPAR northern blot was included as a control for the cytokines used. (**C** and **F**) Ethidium bromide-stained gels show equal amounts of RNA used. Data shown are representative of those obtained in two or three separate experiments, with similar results.

Growth factors and inflammatory cytokines induce expression of VCIP

To examine VCIP expression by other cell types, endothelial, smooth muscle and epithelial cells (A431) were stimulated in monolayer with various growth factors and cytokines for 6 h. Total RNA was then isolated and subjected to northern blot analysis for VCIP and uPAR, as shown in Figure 2. Human dermal microvascular endothelial cells (HdMVECs) responded to most cytokines, but not to EGF. VCIP was expressed most strongly in cells that were stimulated with VEGF (Figure 2A, lane 2). Neither PMA nor $VEGF^{165}$ induced expression of VCIP in carotid artery smooth muscle cells (CASMCs), whereas $VEGF^{165}$ increased VCIP levels in aortic smooth muscle cells (AoSMC), but PMA did not. VCIP levels were strongly induced by PMA and EGF in epidermoid carcinoma (A431) cells, whereas TNFα and bFGF had no effect in this cell type. The uPAR probe was included as a control for cytokines used (Figure 2B and E).

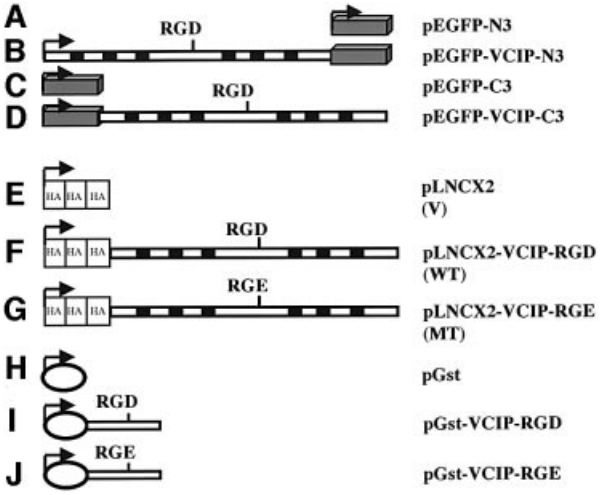

Fig. 3. Schematic diagram of various recombinant cDNA constructs used in this study. (**A**–**D**) pEGFP-based constructs; (**E**–**G**) pLNCX2 retroviral constructs; (**H**–**J**) pGST-fusion protein constructs. The relative positions of RGD and RGE within the constructs are indicated. HA indicates hemaglutinin epitope tags. All constructs are shown in the 5′–3′ orientation. Arrows indicate the direction of transcription.

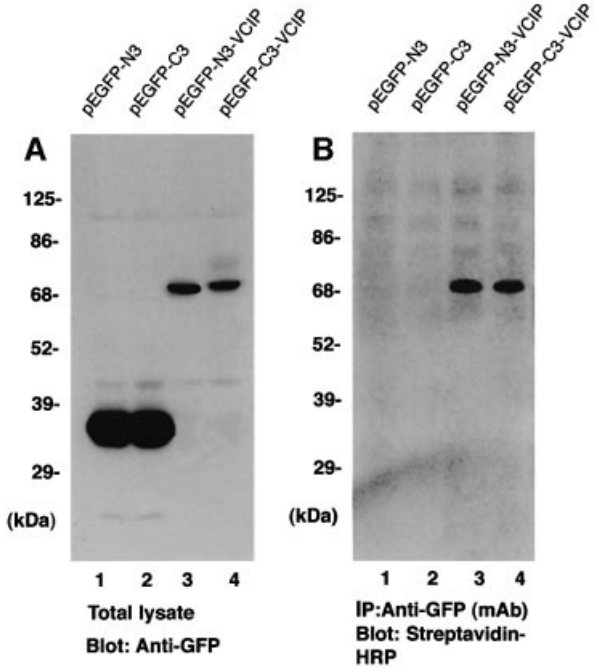

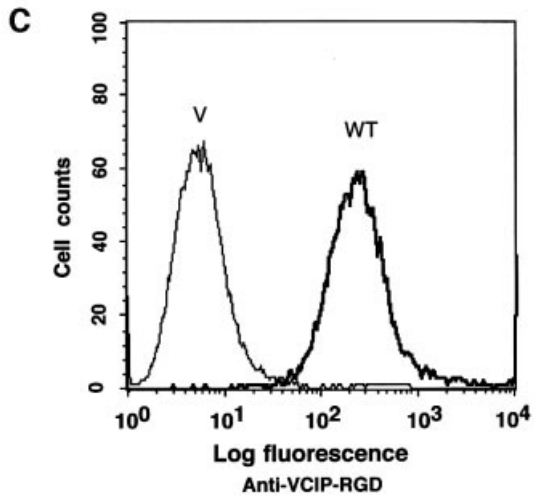

Fig. 4. VCIP is a cell surface antigen. HEK293 cells were transiently transfected with the indicated constructs and subjected to cell surface biotinylation. Cell extracts were subjected to (**A**) anti-GFP immunoblotting or (**B**) immunoprecipitation with anti-GFP monoclonal antibodies followed by streptavidin–HRP immunoblotting. (**C**) FACS analyses of HEK293 cells stably expressing the V or WT constructs. Both cells were stained with anti-VCIP-RGD pAb (30 μg/ml) followed by FITC-labeled anti-rabbit IgG antibodies. Data shown are representative of those obtained in at least three separate experiments, with similar results.

VCIP is a cell surface protein

Using confocal microscopy, Ishikawa *et al*. (2000) showed that PAP2b is localized at the plasma membrane in transfected cells. To determine whether VCIP is a plasma membrane protein that is exposed on the cell surface, HEK293 cells were transfected with green fluorescent protein (GFP)–VCIP fusion proteins. A diagram of the constructs is shown in Figure 3. Transfected cells were detached from culture dishes and subjected to cell surface biotinylation. Proteins were subjected to immunoblotting or immunoprecipitation with anti-GFP antibodies. Cells transfected with the control GFP vector exhibited a ~30 kDa GFP-immunoreactive band (Figure 4A, lanes 1 and 2), whereas a GFP-immunoreactive band of ~68 kDa was detected in lysates from cells transfected with the GFP–VCIP expression vector (Figure 4B, lanes 3 and 4). No biotinylated proteins were detected in anti-GFP immunoprecipitates from HEK293 transfected with vector alone (Figure 4B, lanes 1 and 2), whereas the anti-GFP antibody immunoprecipitated a ~68 kDa biotinylated polypeptide from cells transfected with the pEGFP-VCIP-N3 or -C3 expression vectors (Figure 4B, lanes 3 and 4). Subsequent immunoprecipitation and immunoblot analysis of cell lysates obtained from HUVECs and HdMVECs showed that the M_r of non-glycosylated VCIP is ~38 kDa and that *N*-glycosylated VCIP is 44/48 kDa. Incubation of the VCIP antigen–antibody complex with *N*-glycanase removed the carbohydrate moiety, and the glycosylated forms of this protein were not detectable (data not shown). Furthermore, as shown in Figure 4C, fluorescence-activated cell sorting (FACS) analysis showed that the VCIP-RGD sequence is located outside of the cell surface of 293HEK cells.

Retroviral transduction of VCIP promotes cell–cell interactions

Does VCIP-RGD act as an adhesion ligand? To answer this question, we evaluated the effects of expression of wild-type VCIP (RGD) versus mutant VCIP (RGE) in a cell system that allowed us to study the role of the VCIP-RGD sequence. Primary ECs were not considered suitable for generating stable clones, therefore, we used HEK293 cells to create stable cell lines. HEK293 cells were chosen because they are easily transfected and do not express endogenous VCIP protein. cDNA constructs encoding the various retroviral VCIP constructs were generated (Figure 3E–G). Several clones of HEK293 cells stably expressing wild-type VCIP (pLNCX2-VCIP-RGD-HEK, WT), mutant VCIP (pLNCX2-VCIP-RGE-HEK, MT), or

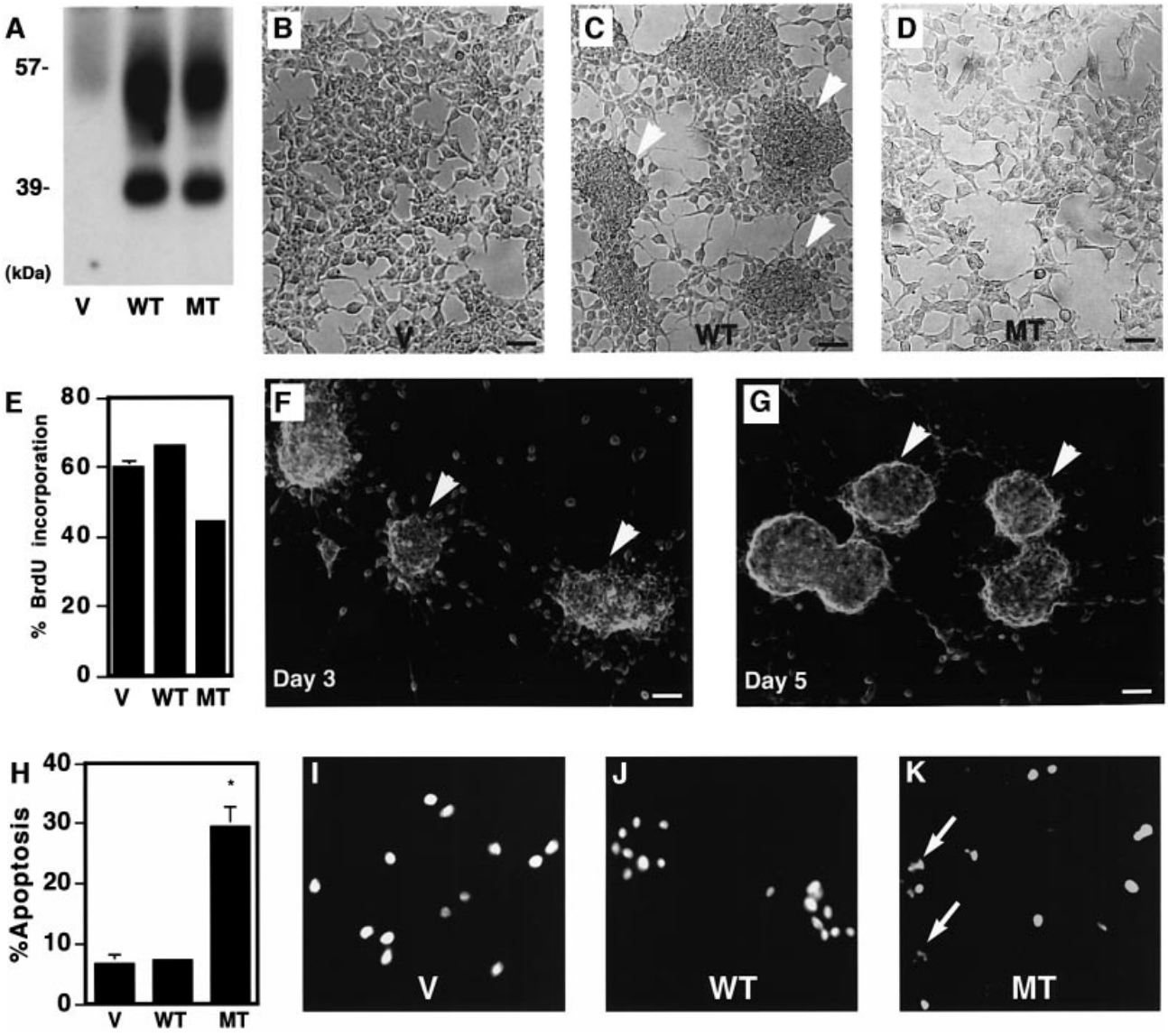

Fig. 5. VCIP promotes cell–cell interactions. (**A**) HEK293 cells were retrovirally transduced with either pLNCX2 (V cells), pLNCX2-VCIP-RGD (WT cells) or pLNCX2-VCIP-RGE (MT cells) and were then propagated in medium containing G418 (500 μg/ml). Clarified cell extracts were immunoprecipitated with affinity purified anti-VCIP-c-cyto rabbit polyclonal antibodies and analyzed by anti-HA immunoblotting. 2×10^5 cells were deprived of growth factors and plated for 36 h in defined medium: (**B**) V cells, (**C**) WT cells, and (**D**) MT cells. Photomicrographs revealed the presence of cell aggregates (indicated by arrowheads) after 12–24 h in WT cells, but not in V or MT cells. (**E**) BrdU uptake was used to measure cell proliferation in V, WT and MT cells. Data are expressed as mean ± SD from triplicate samples. All experiments were performed at least three times. (**F**) High-resolution photomicrographs of live WT cell aggregates after 3 days or (**G**) 5 days. (**H**) The percentage of apoptotic nuclei was determined by scoring at least 300 cells from five randomly selected microscopic fields. Data are expressed as the mean ± SD from triplicate samples. Representative photomicrographs of Hoechst-stained (**I**) V, (**J**) WT and (**K**) MT cells; apoptotic nuclei are indicated by arrows (K). Magnification, 100×. Bar, 25 μm. *, $P < 0.05$.

vector alone (pLNCX2-HEK, V) were obtained under geneticin (G418) selection (see Materials and methods). Three independent clones were isolated for each construct, to ensure that any observed effects were not due to phenotypic variability intrinsic to cultured cells. Clones were regularly evaluated by semi-quantitative RT–PCR (20 cycles) and by immunoblotting to ensure that mRNA and protein expression levels were not altered (data not shown). pLNCX2-HEK (V) was chosen as a control because it is has no known effect on cells. Cell lysates were subjected to immunoprecipitation with an anti-VCIP-cyto antibody, and analyzed by anti-hemaglutinin (HA) immunoblotting. WT and MT cells expressed equivalent levels of VCIP immunoreactivity (Figure 5A). We observed that WT cells formed cell–cell contacts (cell aggregates), whereas MT and V cells did not (Figure 5B–D). The rate of formation of cell aggregates in WT cells was dependent on the number of cells seeded. When 2×10^5 cells were seeded sparsely in a 35 mm dish, the formation of cell aggregates was relatively slow (data not shown). In fact, when WT cells were seeded sparsely, they underwent at least one cell division prior to forming such cell aggregates. The formation of cell aggregates accelerated when 5×10^7 cells were initially seeded (data

Table I. Cell aggregation

HEK cells stably expressing		Substance	Concentration	% cell aggregates
pLNCX2 (vector alone)	(V)	–	–	0
pLNCX2-VCIP-RGD	(WT)	–	–	94 ± 5.5[a]
pLNCX2-VCIP-RGE	(MT)	–	–	0
pLNCX2-VCIP-RGD	(WT)	Anti-rabbit IgG	25 μg/ml	90 ± 7.3
pLNCX2-VCIP-RGD	(WT)	Anti-rabbit IgG	50 μg/ml	91 ± 8.8
pLNCX2-VCIP-RGD	(WT)	Anti-VCIP-RGD	25 μg/ml	73 ± 7.4
pLNCX2-VCIP-RGD	(WT)	Anti-VCIP-RGD	50 μg/ml	36 ± 12.5[a]
pLNCX2-VCIP-RGD	(WT)	NYCRGDDSK	10 nM	67 ± 15.7
pLNCX2-VCIP-RGD	(WT)	NYCRGDDSK	30 nM	46 ± 13.3
pLNCX2-VCIP-RGD	(WT)	NYCRGDDSK	50 nM	28 ± 10.5[a]
pLNCX2-VCIP-RGD	(WT)	NYCRADDSK	10 nM	92 ± 5.7
pLNCX2-VCIP-RGD	(WT)	NYCRADDSK	30 nM	89 ± 7.5
pLNCX2-VCIP-RGD	(WT)	NYCRADDSK	50 nM	90 ± 7.2[a]

2.0×10^5 HEK cells were pre-treated with indicated substance, washed with PBS, plated in defined media and allowed to form cell aggregates at 37°C. This experiment was carried out using 12-well tissue culture plates. Fresh aliquots of substances were added every 12 h. The number of cell aggregates formed was enumerated at the end of 48 h. Typically, 8–12 cell aggregates were visible in a single 100× microscopic field. At least 5–7 random fields were selected. Experiments were performed three times in triplicate. Values represent mean ± SD.
[a]$P < 0.05$.

not shown). As the time in culture progressed, cell aggregates of various sizes were visually recognizable within 24–36 h of seeding (Figure 5C). Cell aggregates continued to grow in size until 98 h or longer. As the colonies increased in size, most of the surrounding cells migrated (relocated) and adhered to the growing cell mass. Eventually, the colonies grew to a sufficiently large size so that they detached from the dishes.

WT cells were also incubated with several peptides modeled after the VCIP-RGD region. When WT cells were cultured in the continuous presence of an anti-VCIP-RGD antibody (25–50 μg/ml) and NYRC**RGD**DSK (10–50 nM), the size, the speed of formation and the number of such cell aggregates were reduced (Table I). In contrast, no reduction in cell aggregation was observed in cells incubated with the mutant peptides NYRC**RAD**DSK (10–50 nM) or NYRC**RGE**DSK (10–50 nM). Incubation with the antibody or peptides did not induce toxicity or cell death. The cell aggregation observed in WT cells was specific, in that cells transfected with pLNCX2-HEK or pLNCX2-VCIP-RGE-HEK did not exhibit such phenotype (Figure 5B and D). In order to eliminate the possibility of clonal variation, three independent clones of WT cells were examined. This phenotype was also reproduced in NIH 3T3 cells under similar experimental conditions. High resolution photomicrographs of living cell cultures demonstrated the progressive formation of cell aggregates by WT cells at days 3 and 5, as shown in Figure 5F–G. In addition, three different clones of WT cells embedded in soft agar supplemented with complete media failed to show anchorage-independent cell growth or colony formation.

Next, we examined the ability of VCIP proteins to regulate proliferation and apoptosis in HEK293 cells. As shown in Figure 5E, WT cells were clearly proliferation competent, as VCIP expression increased the number of BrdU-positive cells by ~65%, which was comparable to the number of BrdU-positive cells in control (V) cells (~60%). In parallel, cells were incubated in defined media and apoptosis was evaluated after 36 h (Figure 5H). Interestingly, MT cells showed the highest levels of apoptosis (~25% of all nuclei were apoptotic), whereas V and WT cells exhibited only baseline levels of apoptosis (~6–8%). Representative photomicrographs of Hoechst-stained cells are shown in Figure 5I–K.

VCIP-mediated signaling

Next, we asked how the expression of VCIP influences the growth properties of HEK293 cells. To identify the molecular events associated with pLNCX2-VCIP-RGD-HEK cell–cell interactions, we measured β_1 integrin and p120catenin (p120ctn) protein levels. We also measured the phosphorylation state and total protein levels of the Fak, Akt, GSK3β and Erk2 protein kinases, which play roles in adhesion-mediated cell proliferation, survival and migration. Enzymatic activation of these protein kinases is accompanied by an increase in phosphorylation state. β_1 integrin immunoreactivity levels were similar in V, WT and MT cells (Figure 6A). Interestingly, p120ctn immunoreactivity levels were increased in WT cells, as compared with V or MT cells. Similarly, the phosphorylation state of Fak, Akt and GSK3β were increased in WT cells, as compared with V or MT cells (Figure 6C, D and G). The phosphorylation state of Erk1/2 was only modestly increased in WT cells, as compared with the dramatic increase in phosphorylation state of Akt in WT cells (Figure 6D and F). In contrast, the phosphorylation state of Jnk was not different in WT and V cells, but was moderately increased in MT cells (Figure 6E). In MT cells, a relative decrease in the phosphorylation of Akt (Figure 6D), together with a moderate increase in the phosphorylation state of Jnk (Figure 6E), may contribute to the higher levels of apoptosis observed in these cells (Figure 5H). There were no differences in the total levels of Fak, Akt, Jnk, Erk 1/2 or GSK3β proteins in V, WT and MT cells. Similarly, we did not observe any differences in the level of expression of β-catenin, γ-catenin and pan-cadherin by western blotting analyses in any of these cells (data not shown).

VCIP promotes direct cell–cell interactions

Because expression of WT, but not MT induced spontaneous 'cell–cell interactions' (cell aggregation) in

293HEK cells, we hypothesized that VCIP-RGD could act as a cell-associated integrin ligand. Thereby, VCIP-RGD could promote 'cell–cell interactions' by specifically recognizing $\alpha_v\beta_3$ and $\alpha_5\beta_1$ integrins presented on adjacent cells.

As shown in Figure 7, the mixing of WT cells with MT cells (0.5×10^6) resulted in the formation of at least 10–15 small and large aggregates within 6 h. These interactions were effectively inhibited by pre-incubating WT cells with an anti-VCIP-RGD antibody, but not with control antibodies. Similar results were obtained when WT cells were incubated with the GRGDSP (25 μM) peptide or the anti-VCIP-RGD antibody (Figure 7D and E). Dose-dependent inhibition of cell aggregates in response to the GRGDSP peptide and anti-VCIP-RGD antibody are shown in Figure 7F.

Since, 293HEK cells express high level of $\alpha_5\beta_1$, but somewhat relatively low in $\alpha_v\beta_3$ integrin heterodimer, we mixed WT cells with cells expressing high levels of the β_3 integrin subunit to evaluate the effects on cell aggregation. 293HEK cells were stably transfected with the wild-type human β_3 integrin subunit. Expression levels were determined by FACS and western analyses. Mixing of WT cells with β_3 integrin–293HEK cells quickly resulted in significant cell aggregation within 3–6 h (data not shown).

VCIP interacts with $\alpha_v\beta_3$ and $\alpha_5\beta_1$ integrins

In view of these findings, we directly examined whether recombinant VCIP expression could promote adhesion of ECs in primary culture. In order to determine whether the VCIP-RGD motif acts as an integrin ligand, we generated two recombinant VCIP fragments (each 49 amino acids in length) that corresponded to a predicted second extracellular loop of the protein (Figures 1L and 3H–J). Wild-type glutathione *S*-transferase (GST)–VCIP-RGD and mutant GST–VCIP-RGE fusion proteins were affinity purified and visualized by Coomassie Blue staining on SDS–PAGE, as shown in Figure 8A. Both the wild-type and mutant proteins migrated at the predicted size of 34 kDa. To determine whether GST–VCIP-RGD could interact with various integrins, a solid-phase ligand binding assay was performed. The assay was carried out as described by Orlando and Cheresh (1991), with minor modifications. As shown in Figure 8B, the $\alpha_5\beta_1$ and $\alpha_v\beta_3$ integrin heterodimers interacted with GST–VCIP-RGD in solution with comparable affinities, whereas the $\alpha_2\beta_1$ and $\alpha_v\beta_5$ integrins did not. None of these integrins significantly interacted with GST alone or with the GST–VCIP-RGE mutant, suggesting that the interaction of VCIP-RGD with $\alpha_5\beta_1$ and $\alpha_v\beta_3$ integrins is highly specific. VCIP-RGD bound to $\alpha_v\beta_3$ integrin in a dose-dependent manner, whereas GST alone or GST–VCIP-RGE exhibited negligible binding to $\alpha_v\beta_3$ integrin (Figure 8C). Representative photomicrographs of optimal adhesion and spreading of ECs plated for 45 min on fibronectin, vitronectin and GST–VCIP-RGD are shown in Figure 8D–F. Adhesion of

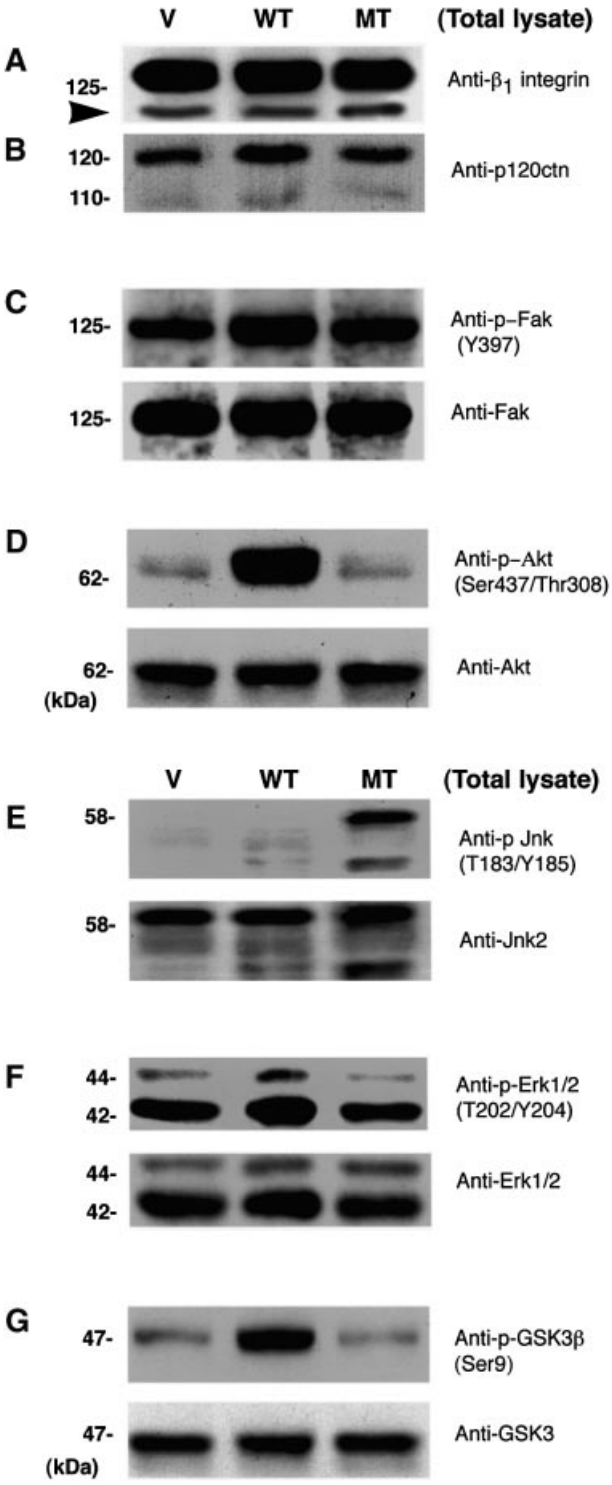

Fig. 6. VCIP-induced regulation of various intracellular signaling pathways. Cells were cultured exactly as described in Figure 5. At the end of 36 h, V, WT and MT cells were solubilized, and extracts analyzed by immunoblotting with the indicated antibodies. Phospho-specific immunoblots were stripped and re-probed with the corresponding total antibodies, to confirm that equal amounts of protein were loaded across the lanes, as shown. (**A**) β_1 integrin immunoblot. Arrowhead indicates immature form of the β_1 integrin subunit. (**B**) p120ctn immunoblot. HEK293 cells express two isoforms of p120ctn, isoform-1 (p120) and isoform-2 (p110); p110 is less abundant in HEK293 cells. (**C**) Phospho-FAK and total FAK immunoblots. (**D**) Phospho-Akt and total Akt immunoblots. (**E**) Phospho-Jnk and total Jnk immunoblots. (**F**) Phospho-Erk1/2 and total Erk1/2 immunoblots. (**G**) Phospho-GSK3β and total GSK3β immunoblots. All blots shown are representative of those obtained in at least three separate experiments, with similar results.

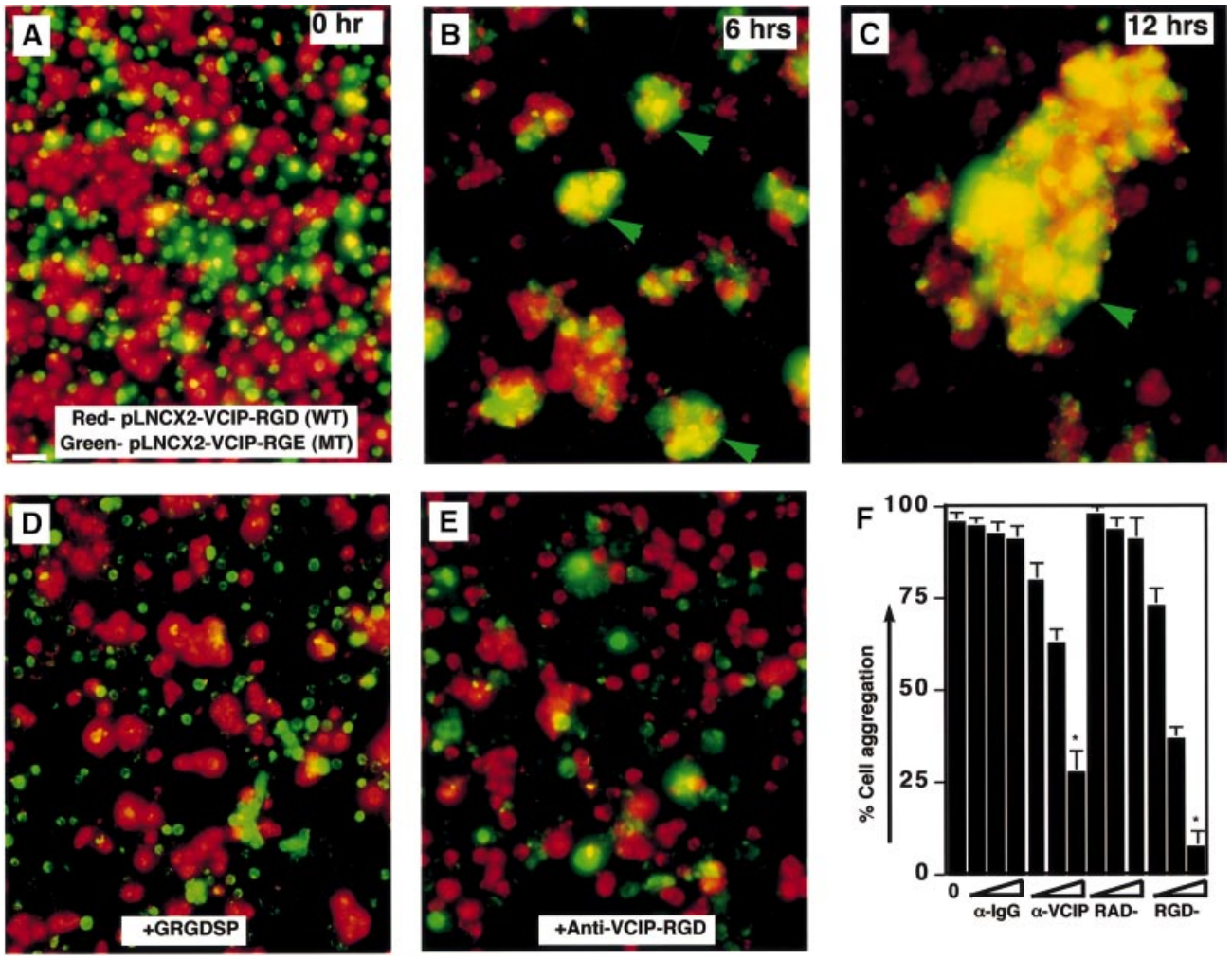

Fig. 7. VCIP mediates heterophilic cell–cell interactions. (**A**) Representative photomicrograph of a mixture of WT and MT cells labeled with red (DiI) and green (DiO) fluorescent dyes at 0 h. (**B**) Small and large cell-aggregates were visible after 6 h; green arrowheads indicate the most productive cell aggregation (yellow). (**C**) Representative large cell aggregates are shown after 12 h. (**D**) Cells co-incubated with the GRGDSP peptide for 12 h. (**E**) Cells co-incubated with anti-VCIP-RGD antibody (25 μg/ml) after 12 h. All experiments were performed at least three times in triplicates. (**F**) Histogram showing that the anti-VCIP-RGD (α-VCIP) antibody and GRGDSP (RGD–) peptides dose-dependently inhibited cell aggregation, whereas control antibodies (α-IgG) and peptides GRADSP (RAD–) did not. Magnification, 200×. Bar, 40 μm. *, $P < 0.05$. The images of cell aggregates appear out of focus.

ECs to GST–VCIP-RGD was comparable to that observed in wells coated with vitronectin and fibronectin substrates.

Next, we evaluated the capacity of VCIP-RGD to bind EC integrins, by determining the effect of GST–VCIP fusion proteins on cell adhesion and spreading. ECs adhered to wells coated with recombinant wild-type GST–VCIP-RGD protein in a dose-dependent manner. In contrast, there was little adhesion to wells coated with the mutant (GST–VCIP-RGE) fusion protein (Figure 8G). Active protein synthesis was not required for ECs to attach to the substrates we tested, because pre-treatment of ECs with cycloheximide (20 μg/ml) for 1 h prior to replating the cells onto substrate-coated dishes followed by continued exposure to cycloheximide during the entire assay period did not decrease the total number of attached cells (data not shown).

Next, we sought to determine which integrin(s) actually mediated adhesion to the VCIP-RGD sequence. To do so, ECs were non-enzymatically detached from dishes, washed, pre-incubated with various blocking antibodies and washed again to remove unbound antibodies. ECs were resuspended in serum-free M199 media and immediately replated onto GST–VCIP-RGD-coated wells. Pre-incubation of ECs with anti-$\alpha_5\beta_1$ (P1D6) and anti-$\alpha_v\beta_3$ (LM609) antibodies inhibited the attachment of ECs in a dose-dependent manner (Figure 8G). Control anti-$\alpha_2\beta_1$ (MAB 1998) and anti-$\alpha_3\beta_1$ (P1B5) integrin function-blocking antibodies did not have any effect on adhesion of ECs to GST–VCIP-RGD. When ECs were co-incubated with a mixture of P1D6 (10 μg/ml) and LM609 (10 μg/ml), cells remained rounded, indicating that adhesion of these cells to GST–VCIP-RGD was completely inhibited. In contrast, when applied alone, neither of these two antibodies completely inhibited the adhesion of ECs (data not shown). It is possible that $\alpha_v\beta_1$, $\alpha_v\beta_5$ and $\alpha_v\beta_6$ integrins may also mediate the interaction between ECs and VCIP-RGD to some extent. Furthermore, adhesion of ECs to VCIP required the presence of Ca^{2+} and Mg^{2+}, as the addition of 2.5 mM EDTA (pH 7.4) for 5 min caused cells to detach from tissue culture dishes. In addition, when the acetylated NYRC**RGD**DSKVQE (VCIP-RGD) peptide was incubated with attached cells (i.e. cells that

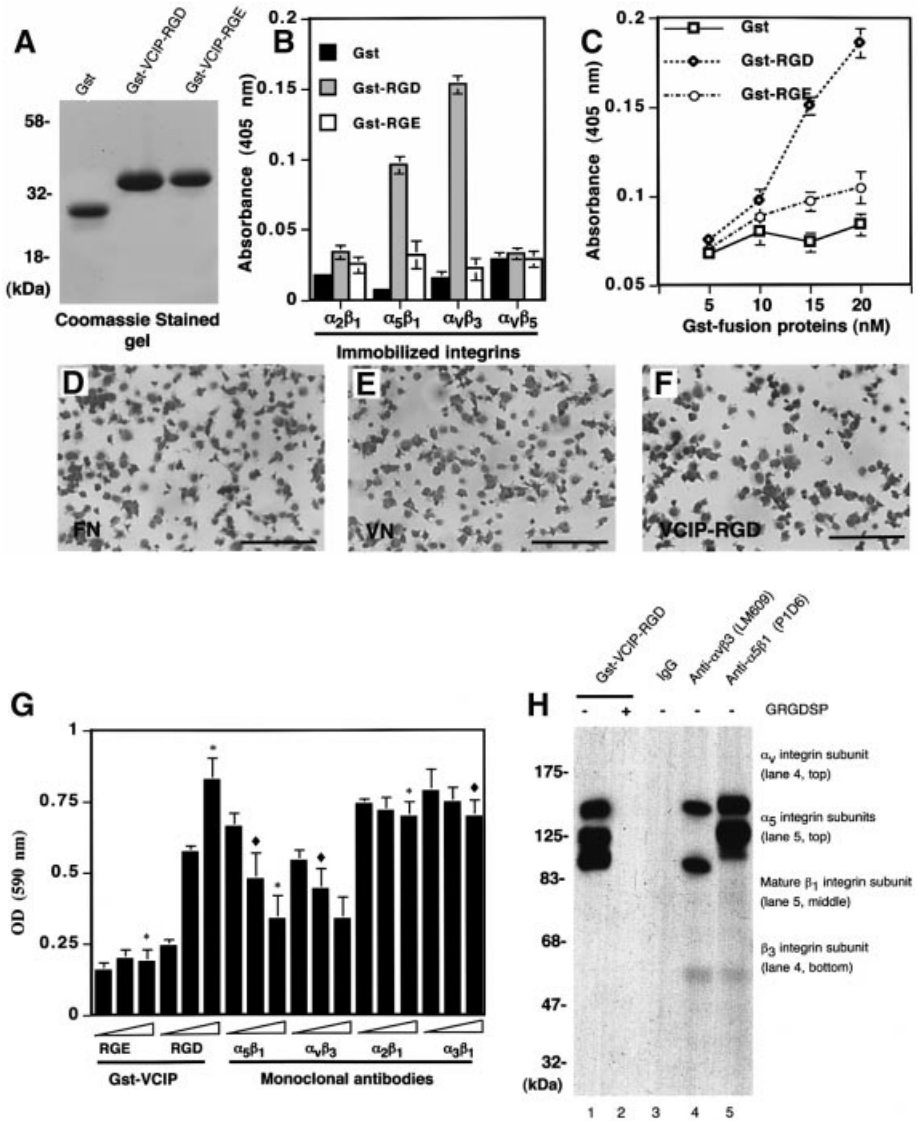

Fig. 8. Recombinant expression of the VCIP-RGD protein induces interactions with $\alpha_v\beta_3$ and $\alpha_5\beta_1$ integrins. (**A**) Affinity purified GST-fusion proteins were resolved on SDS–PAGE and stained with Coomassie Blue. (**B**) Integrins were immobilized onto 96-well plates, and the various GST-fusion proteins (ligands) were allowed to bind. Bound ligands were incubated with anti-GST antibodies, appropriate substrate added and the color intensity measured. OD values <0.05 were considered to be background binding. Data are expressed as mean ± SD (n = 4). (**C**) Dose-dependent binding of $\alpha_v\beta_3$ integrin with recombinant GST–VCIP-RGD. Representative photomicrographs of adhesion and spreading of ECs replated onto dishes coated with either (**D**) fibronectin (Fn), (**E**) vitronectin (Vn) or (**F**) GST–VCIP-RGD. Cells were allowed to attach for 45 min, washed with PBS and stained with H&E. Magnification, 100×. Bar, 25 μm. (**G**) Adhesion blocking assays. ECs were replated onto dishes coated with increasing concentrations of affinity purified fusion proteins (1, 5 and 10 nM). Attached cells were stained, washed and absorbances of eluted dyes measured. To determine the effects of anti-integrin antibodies, dishes were coated with 10 nM GST–VCIP-RGD. ECs were pre-incubated at 4°C with increasing concentrations of anti-$\alpha_5\beta_1$ (P1D6), anti-$\alpha_v\beta_3$ (LM609), anti-$\alpha_2\beta_1$ (MAB 1998) and anti-$\alpha_3\beta_1$ (P1B5) monoclonal antibodies (1, 5 and 10 μg/ml) for 30 min, then washed and replated onto coated dishes. Attached cells were stained, washed and absorbances of eluted dyes determined. Three independent experiments were performed with several replicate samples in each experiment. Data are expressed as mean ± S.D.; diamond, P <0.01; asteisk, P <0.001. (**H**) Clarified extracts prepared from [^{35}S]Cys/Met-labeled HdMVEC were pre-adsorbed and incubated with GST–VCIP-RGD in the absence (–) or presence (+) of GRGDSP peptide (lanes 1 and 2). The presence of $\alpha_v\beta_3$ and $\alpha_5\beta_1$ integrins (lanes 5 and 6) in GST–VCIP pull-down complex (lane 1) was confirmed by incubating aliquots of dissociated complex with the indicated antibodies, as described in Materials and methods. Anti-mouse IgG was included as negative control (lane 3).

were plated on VCIP-RGD-coated wells) at a concentration of 5 nM, cells rounded up within 5 min and eventually completely detached from the wells.

Recombinantly expressed VCIP interacts directly with $\alpha_5\beta_1$ and $\alpha_V\beta_3$ integrins

To confirm that VCIP-RGD interacts with integrins, clarified cell lysates were obtained from [^{35}S]Met/Cys labeled HUVECs and subjected to affinity chromatography. Lysates were pre-adsorbed twice with GST–Sepharose beads to remove proteins that interact with GST–Sepharose beads non-specifically. Pre-adsorbed lysates were incubated with GST–VCIP-RGD fusion proteins (10 μg per 3 mg lysate) in the presence or absence of GRGDSP (25 μM). The beads were then extensively washed. To determine whether integrins were present in the GST–VCIP-RGD pull-down complex, the contents of a tube that did not receive the GRGDSP

peptide was boiled in a dissociation buffer containing 0.5% SDS. The samples were equally divided into three tubes and diluted with cold immunoprecipitation dilution buffer to adjust the concentration of SDS to <0.1%. The samples were then immediately subjected to immunoprecipitation with indicated antibodies (Figure 8H). We found that the GST–VCIP-RGD pull-down complex indeed contained anti-$\alpha_v\beta_3$ and -$\alpha_5\beta_1$ immunoreactivities (Figure 8H, lanes 4 and 5).

Adhesion of ECs through VCIP-RGD induces integrin-mediated signaling

Adhesion of cells to ECM proteins promotes clustering of integrins at the plane of the plasma membrane. In addition to promoting structural support, this event nucleates formation of a complex of signaling-competent intracellular proteins (Schlaepfer *et al*., 1994; Wary *et al*., 1996, 1998; Pozzi *et al*., 1998). To investigate whether adhesion of cells to VCIP-RGD results in tyrosine phosphorylation of key focal adhesion signaling proteins, p125FAK, p46/52Shc, p130Cas and paxillin were immunoprecipitated and subjected to immunoblotting with various phospho-specific antibodies. Serum- and growth factor-starved HUVECs were allowed to attach and spread on dishes coated with optimal concentrations of fibronectin (Fn), vitronectin (Vn), GST–RGD-VCIP and GST–VCIP-RGE. Cells were harvested after 30 and 60 min at 37°C. Cells were then solubilized, clarified, pre-adsorbed, immunoprecipitated and subjected to immunoblotting with various antibodies, as shown in Figure 9. VCIP-RGD induced tyrosine phosphorylation of Fak, Cas, Shc and paxillin at both 30 and 60 min. The signal intensities induced by expression of GST–VCIP-RGD were comparable to those induced by Fn and Vn. In contrast, GST–VCIP-RGE did not induce detectable tyrosine phosphorylation of Fak, Cas, Shc or paxillin. Cells that were replated onto GST–VCIP-RGE appeared rounded. Stripping and reprobing blots with anti-p125FAK, anti-p130Cas, anti-Shc and anti-paxillin antibodies showed that equal amounts of these proteins were present under all experimental conditions (data not shown).

Co-expression of VCIP with vWF and $\alpha_v\beta_3$ integrin in tumor vasculature

Angiogenesis is required for the growth and survival of all solid tumors (Hanahan and Folkman, 1996; Carmeliet and Jain, 2000). To determine whether VCIP was expressed and co-localized with known angiogenic markers in tumor vasculatures, we immunostained tumor sections with an anti-VCIP-RGD antibody. The specificity of affinity-purified anti-VCIP-RGD was confirmed by ELISA, western immunoblotting and immunolabeling experiments (data not shown). Anti-VCIP-RGD reacted specifically with the GST–VCIP-RGD fusion protein, but did not react with GST–VCIP-RGE or GST alone. Moreover, the anti-VCIP-RGD antibody did not react with other RGD-containing ECM molecules, such as Fn, Vn or type I collagen (data not shown). Because the antibody did not cross-react with mouse antigens, we chose to analyze human tissue sections. Tissue sections were initially examined by immunostaining with anti-platelet endothelial cell adhesion molecule-1 (PECAM-1, also known as CD31), anti-VE (vascular endothelial)-cadherin and anti-von Willebrand Factor (vWF) antibodies to establish the presence of endothelium. Paraffin-embedded tumor tissue sections that lacked blood vessels did not exhibit VCIP immunoreactivity. Therefore, we used tumor tissue sections that clearly contained ECs. To examine whether VCIP was expressed in angiogenic tissues, we examined serial sections of skin melanoma, angioma and normal skin tissues. Enriched expressions of VEGF and $\alpha_v\beta_3$ integrin are common in angiogenic tissues, and are associated with invasion and growth of solid tumors (Hoshiga *et al*., 1995; Dufourcq *et al*., 1998). An increase in the levels of vWF expression is considered to be a negative prognostic factor for tumor-induced angiogenesis. Indirect double-immunolabeling experiments showed that VCIP co-localized with vWF and VEGF in vasculatures of skin melanoma tumors (Figure 10). VCIP also clearly co-localized with $\alpha_v\beta_3$ integrin in the angioma tissue sections examined (Figure 10). Normal skin exhibited PECAM-1 (CD31) immunoreactivity, but not VCIP immunoreactivity (Supplementary figure 3). VCIP immunoreactivity was lost when the affinity purified anti-VCIP antibody was incubated with the peptide used to generate the primary antibody, thereby confirming the specificity of this antibody.

Discussion

VCIP is PAP2b

In our search for novel proteins that regulate capillary morphogenesis of ECs, we identified PAP2b/VCIP as an interesting candidate. Here, we identified VCIP/PAP2b mRNA as a 3.4 kb transcript, but not as a 1.6 kb transcript as described previously (Kai *et al*., 1997). We did not detect a 1.6 kb PAP2b transcript in any of our northern blot analyses, regardless of the stringency of washing conditions. The cell membrane fraction prepared from 293T cells overexpressing PAP2b showed phosphatase activity against phosphatidic acid that was independent of Mg^{2+}, insensitive to *N*-ethylmaleimide exposure, and blocked by propranolol and sphingosine (Roberts *et al*., 1998; Ishikawa *et al*., 2000). However, Roberts *et al*. (1998) could not determine PAP2b activity at the surface of intact Sf9 insect cells. Kai *et al*. (1997) showed that EGF exposure enhanced the expression of PAP2b in quiescent HeLa cells, but had no effect on PAP2a mRNA. Our data show VEGF, bFGF and PMA are able to induce expression of VCIP in three dimensional as well as monolayer cells. Cell surface biotinylation and FACS data indicated that VCIP-RGD is located on the cell surface.

VCIP promotes heterophilic cell–cell interactions and signaling

Because VCIP exhibited an RGD sequence, we sought to determine its ability to act as a cell-associated integrin ligand and promote heterophilic cell–cell interactions. Cell–cell interactions contribute to normal as well as unwanted cell cycle progression, vascular malformations, expansion of atherosclerotic lesions, invasion and the growth of solid tumors (Assoian and Marcantonio, 1996; Hanahan and Folkman, 1996; Carmeliet and Jain, 2000; Tailor and Granger, 2000; McEver, 2001). Interestingly, in HEK293 cells, expression of the pLNCX2-VCIP-RGD

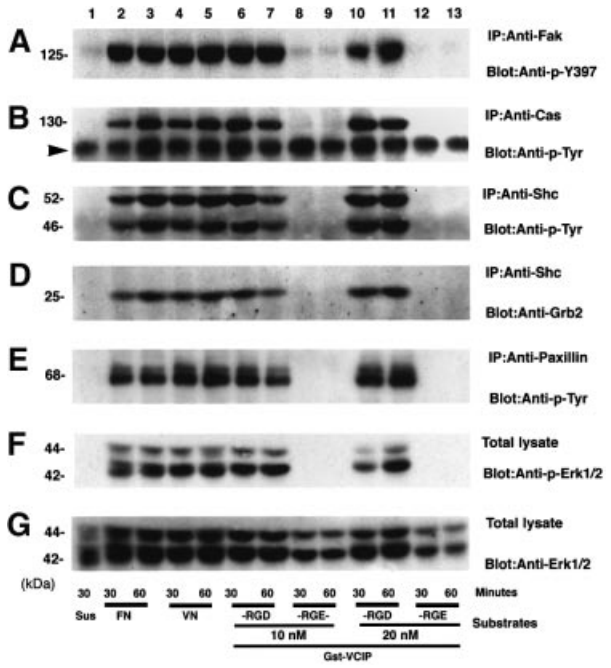

Fig. 9. Tyrosine phosphorylation of Fak, Cas, Shc, Paxillin and Erk2. Dishes were coated with either fibronectin (Fn, 10 μg/ml), vitronectin (Vn, 10 μg/ml) or affinity purified GST–VCIP-RGD or -RGE fusion proteins (10 and 20 nM). ECs were detached, washed and maintained in suspension (Sus) for 30 min, then allowed to re-attach for 30 or 60 min. Adherent cells were solubilized in RIPA buffer. (**A**–**E**) Equal amounts of protein (~1.0 mg) from clarified extracts were subjected to immunoprecipitation (IP) followed by immunoblotting using the indicated antibodies. (**F**) Equal amounts of protein from total lysates (35 μg/lane) were subjected to immunoblotting with the anti-phospho-Erk1/2 antibody. (**G**) The same membrane was stripped and re-probed with an anti-Erk1/2 antibody, showing that equivalent amounts of proteins used across the lanes. Blots shown are representative of those obtained in at least three separate experiments.

(WT) construct induced cell aggregation, whereas control cells remained as monolayer. To determine whether this interaction was mediated by the RGD motif, we passaged WT cells in media containing VCIP-derived peptides and fusion proteins. Addition of these reagents decreased, but did not completely abolish the formation of cell–cell interactions. VCIP expression induced a moderate increase in proliferation of WT cells. Surprisingly, MT cells exhibited higher levels of apoptosis than WT or V cells. This effect is most likely not due to the inability of VCIP-RGE to function as a cell-associated integrin ligand. We speculate that the mutation of RGD (WT) sequence to RGE (MT) may have altered the enzymatic activity of VCIP. This alteration in enzymatic activity may affect the steady-state level of pro-apoptotic molecules such as sphingosine and ceramide (Jasinska *et al*., 1999). One could also suggest that the mutant VCIP (RGD to RGE) is probably somewhat incompatible with the cell growth. Is it possible that compared with the wild type, the mutant form of VCIP could function (i.e. mutant PAP2b with RGE sequence) as a more potent lipid phosphatase enzyme? If so, this could induce loss of active form of lipid signaling molecules such as 'ceramide-1-phosphate' and increase accumulation of pro-apoptotic molecule 'ceramide' (also sphingosine). Currently, we do not have any biochemical evidence to suggest a mechanism. This study will entail phosphatase-dead version of VCIP cDNA constructs.

Cell–cell interactions were associated with a modest increase in the tyrosine phosphorylation state of p125FAK in WT cells. The phosphorylation state, and presumably enzymatic activation, of Akt and Erk2 were also increased in WT cells. These findings suggest increased integrin ligation in WT than in V or MT cells. Interestingly, GSK3β also appeared to be activated moderately in WT cells. The moderate increase in p120ctn (isoform 1) immunoreactivity in WT cells is not clearly understood. Increased phosphorylation of Akt and GSK3β kinases in WT cells is indicative of a survival mechanism already in place to counter impending loss of contact with the substratum. Further studies will be required to fully characterize the signaling mechanisms by which VCIP regulates cell–cell interactions.

The mixing of WT with MT cells also induced cell aggregation. These interactions were specific because anti-VCIP-RGD and GRGDSP peptides blocked cell aggregation, whereas other control substances did not. In addition, cadherin-deficient SW480 cells stably expressing the pLNCX2-VCIP-RGD construct attached to monolayer HUVECs, whereas cells expressing pLNCX2 or pLNCX2-VCIP-RGE did not. Adhesion of pLNCX2-VCIP-RGD-SW480 cells to monolayer HUVECs was blocked by incubation with the anti-VCIP-RGD antibody and the GRGDSP peptide in a dose-dependent manner (Supplementary figure 2), whereas control substances had no significant effect on adhesion.

The specific interactions of VCIP with $\alpha_v\beta_3$ and $\alpha_5\beta_1$ integrins were demonstrated by four complementary approaches. First, the solid phase ligand-binding assay showed that VCIP-RGD, but not VCIP-RGE, bound to $\alpha_v\beta_3$ integrin with slightly higher affinity than to $\alpha_5\beta_1$ integrin (K_D values not shown). These interactions were clearly mediated by the RGD motif and by integrins, because the addition of a soluble NYRC**RGD**DSK peptide during the solid phase assay specifically inhibited these interactions, whereas the mutant NYRC**RGE**DSK or NYRC**RAD**DSK peptides did not. Secondly, pre-incubation with anti-$\alpha_v\beta_3$ and anti-$\alpha_5\beta_1$ integrin adhesion blocking antibodies inhibited attachment of ECs to recombinantly expressed VCIP-RGD. Thirdly, GST–VCIP-RGD was able to capture intact $\alpha_v\beta_3$ and $\alpha_5\beta_1$ integrins from ECs (Figure 8H). Fourthly, VCIP-RGD, but not VCIP-RGE, increased the tyrosine phosphorylation state of the p125Fak, Shc, Cas, paxillin and Erk2 signaling molecules (Figure 9). p125Fak is an intracellular tyrosine kinase, whereas Shc is an adaptor protein that becomes tyrosine phosphorylated in response to integrin clustering and activation of tyrosine kinases. Phosphorylated Shc couples receptor tyrosine kinases and a subset of integrins to the activation of Ras-MEK-Erk2 pathway (Giancotti and Ruoslahti, 1999). The *E.coli* expressed recombinant GST–VCIP-RGD does not have complete catalytic core unit to efficiently function as a lipid phosphatase enzyme. Most lipid phosphatases including glucose-6-phosphatase contain a signature motif KXXXXXXRP-(X12–54)-PSGH-(X31–54)-SRXXXXXHXXXD] (Stukey and Carman, 1997). The recombinant GST–VCIP-RGD protein is composed of 49 amino acid residues (amino acid residues 145–194, Figure 1L); it contains the lipid

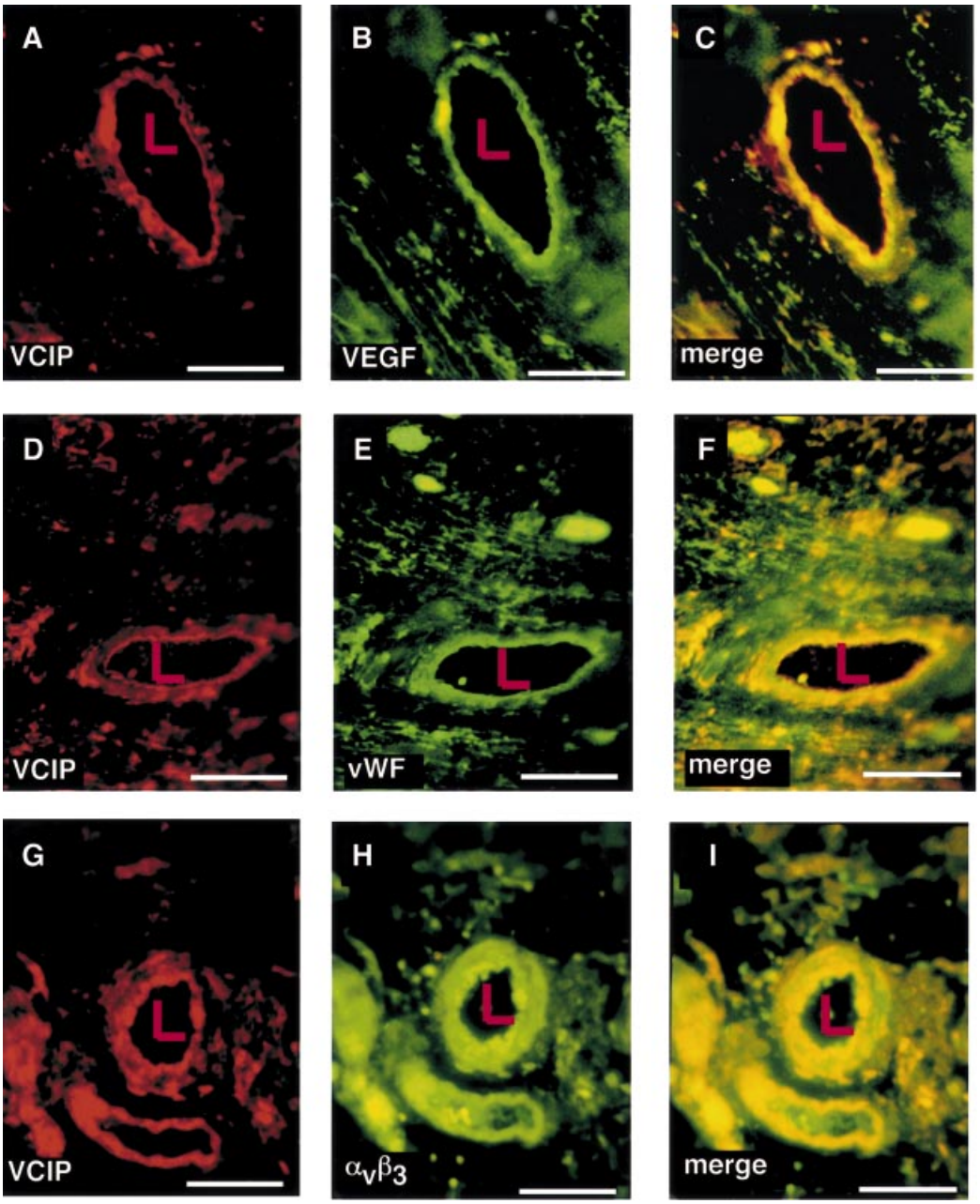

Fig. 10. Co-expression of VCIP with VEGF, and $\alpha_v\beta_3$ integrin in the tumor vasculature. Paraffin-embedded skin melanoma (**A–F**) and angioma (**G–I**) tumor tissue sections (4 μm) were subjected to indirect double immunostaining. The sections were sequentially incubated with affinity purified anti-VCIP-RGD (30 μg/ml) (A, D and G), anti-VEGF (B), anti-vWF (E) or anti-$\alpha_v\beta_3$ integrin (H) monoclonal antibodies. Sections were washed and incubated with goat anti-rabbit IgG conjugated to Texas Red (red) and goat anti-mouse IgG conjugated to FITC (green). Images were taken below the saturation level with a Zeiss Axiovert-125 epifluorescent microscope equipped with a camera. (C), (F) and (I) represent merged images of (A) and (B), (D) and (E), and (G) and (H) respectively. Co-expression and co-incidences are indicated in yellow. Magnification, 100×. L, lumen. Bar, 25 μm.

phosphatase motif (KXXXXXXRP), but lacks a proton donor sequence, i.e., PSGH motif (residue 196–199, Figure 1L) and -(X31–54)-SRXXXXXHXXXD sequence. Taken together, these data suggest that recombinant VCIP-RGD can act as an integrin ligand *in vitro*.

Indirect co-immunostaining of various tumor tissue sections for VCIP and assorted EC markers, including vWF, VEGF and PECAM-1 (CD31) suggested that these proteins are closely co-localized. In contrast, normal skin samples that stained positively for PECAM-1 (CD31) lacked VCIP immunoreactivity (Supplementary figure 3). Most fibroblast and hematopoietic cells examined also lacked VCIP antigen immunoreactivity. Thus, our data suggest that the expression of VCIP may be restricted to vascular cells as well as inflamed and angiogenic tissues.

Physiological relevance of VCIP-mediated cell–cell interactions

What could be the possible physiological relevance of VCIP-mediated cell–cell interactions? Until now, no function other than lipid phosphatase activity has been described for VCIP. Our data clearly show that recombinantly expressed VCIP-RGD molecule can act as an integrin ligand *in vitro*. We also demonstrated that the

intact RGD motif of VCIP is a potent ligand for a subset of integrins. VCIP appears to be preferentially expressed in inflamed/angiogenic tissues. In addition to its known lipid phosphatase activity, we propose that VCIP promotes 'heterophilic interactions', in that it can mediate both 'homotypic' (like) and 'heterotypic' (unlike) cell adhesions. For example, VCIP-RGD could bind monocytes, and thereby enhance the adherence of neutrophils to EC monolayers (Abedi and Zachary, 1995). β_1 and β_2 integrins are known to mediate the adherence of monocytes to endothelial and epithelial cells, an early event in the acute inflammatory response (Luscinskas *et al*., 1994; McEver, 2001; Muller, 2002). It is also possible that activated ECs could recruit carcinoma cells that express VCIP. Alternatively, carcinoma cells such as A431-like cells may utilize VCIP-RGD to recruit activated ECs. Although not tested, we speculate that platelet integrin $\alpha IIb\beta_3$ may also interact with VCIP-RGD and contribute to platelet adhesion and aggregation. Lateral cell–cell interactions may provide a mechanism to impede or stop further migration of cells, thereby sequestering a subset of integrins from the basolateral surface of the cells towards cell–cell junctions. While interactions of ECs with mesenchymal or smooth muscle cells may serve as a mechanism to promote recruitment of mural cells or pericytes, this may also promote maturation of blood vessels (Darland and D'Amore, 2001).

In summary, we have identified a novel function of PAP2b/VCIP. Since synthetic peptide and fusion proteins modeled after the second extracellular loop of VCIP bind selectively to $\alpha_v\beta_3$ and $\alpha_5\beta_1$ integrins, it will be of interest to further investigate the potential for VCIP-derived peptides or proteins to inhibit specific cell–cell interactions. Such inhibitors of cell–cell interactions could be useful for developing novel therapeutic approaches to treat diseases where these interactions have clear pathological consequences, such as inflammation, thrombosis, atherosclerosis, restenosis and tumor-induced angiogenesis. Future experiments will be designed to identify other molecules that may directly or indirectly function with VCIP, and will examine how these factors may influence cell–cell interactions. Such studies will facilitate our understanding of the physiological effects of these molecular interactions.

Materials and methods

Materials

HUVECs, HdMVECs, CASMCs and AoSMCs were obtained from Clonetics. ECM molecules, endotoxin-free fetal bovine serum, antibiotics, heparin, 100× ITS (insulin, transferrin and selenium), M199 media, the anti-$\alpha_5\beta_1$ (P1D6) and anti-$\alpha_3\beta_1$ (P1B5) antibodies and Superscript II reverse transcriptase enzyme were obtained from Invitrogen. Basic fibroblast growth factor (bFGF) and human recombinant vascular endothelial growth factor (hrVEGF^{165}) were purchased from R&D systems. The bovine skin-derived type I collagen (3.0 mg/ml) solution was purchased from Cohesion Inc. Multiple tissue northern blot, cDNA amplification kit and the human placental cDNA library in λTriple-Ex vector were purchased from Clontech Laboratories, Inc. Anti-phospho-specific antibodies were purchased from New England Biolabs. Hybridomas producing the anti-human $\alpha_1\beta_1$ integrin antibody (clone TS2/7) were obtained from ATCC, and the purified antibody is available from our laboratory. The anti-$\alpha_2\beta_1$ (MAB 1998), anti-$\alpha_v\beta_3$ (LM609) and VE-cadherin (MAB1989) antibodies were procured from Chemicon. The mouse anti-p120catenin (clone 15D2) monoclonal antibody was obtained from Zymed Laboratories, Inc. Synthetic peptides LSPVDIIDRNNHHNM and EGYIQNYRCRGDDSKVQEAR were used to raise anti-VCIP-cyto-C16 and anti-VCIP-RGD antibodies, respectively (Alpha Diagnostic International). These antibodies were affinity purified prior to use (Harlow and Lane, 1988).

Monolayer and three-dimensional cell culture

Monolayer cell cultures were carried out as described previously (Wary *et al*., 1996; Thakker *et al*., 1999). Three-dimensional matrix gel was prepared by gently mixing a cold solution of bovine skin-derived type I collagen solution (2.1 mg/ml) with media M199, 1× ITS, hrVEGF^{165} (100 μg/ml) and glutamine (2.4 mM). The pH was adjusted to 7.5 with 0.1 N sodium hydroxide and sterile water was used to adjust the final volume. Proliferating ECs in the third or fourth passage were cultured in complete media and gently resuspended in complete M199 media at a concentration of 4×10^5 cells/ml. 24-well tissue culture dishes were filled with 300 μl of cold 3D gel solution, and placed at 37°C in a CO_2 incubator for 30–45 min to polymerize and solidify. Resuspended cells (2×10^5 cells in 500 μl) were seeded onto 3D gel and dishes returned to the CO_2 incubator at 37°C to allow the cells to attach for 2–3 h. At the end of this period, unattached cells were removed, and a second layer of 3D gel was poured that included M199 media supplemented with 20% adult human serum-AB and 2.4 mM L-glutamine, in the presence or absence of 100 ng/ml human recombinant VEGF^{165}. Thus, ECs were grown embedded between two layers of type I collagen gel. To induce capillary morphogenesis of ECs, 3D gels were filled with 500 μl of tubulogenic media, including M199 media, 1× ITS, 20% adult human serum-AB and hrVEGF^{165} (100 ng/ml). The term 'tubulogenic media' is used to describe the media that induces formation of 'capillary (or tubule) morphogenesis' of ECs grown in 3D gels.

cDNA library screening, northern blot analysis, PCR and RT–PCR

A λTripleEx phage cDNA library prepared from human placenta (Clontech) was screened as described previously (Wary *et al*., 1993). Plasmids were extracted, purified by Qiagen affinity column and then digested with *Eco*RI and *Xba*I to confirm the presence of the insert. Six overlapping clones were subjected to DNA sequencing. All northern blot analyses were performed as described previously (Wary *et al*., 1993). In brief, 20 μg of total RNA or 2 μg poly(A)$^+$ mRNA from control cells (i.e. ECs embedded in three-dimensional type I collagen in presence of 20% human adult serum-AB ± 100 ng/ml hrVEGF^{165} supplied every 6 h) were fractionated on an agarose gel containing formaldehyde. To analyze various mRNA levels by RT–PCR, the following primers were used: VCIP-forward 5′-GGAGGATCCCTCGCGCCGCAGCCAGCGCCATGC-3′ and -reverse 5′-GTGGCACCTACATCATGTTGTGGTG-3′; human uPAR-forward 5′-CTTCCTGAAATGCGTCAACACC-3′ and -reverse 5′-TCATAGCTGGGAAAACTGAGGC-3′ (accession No. X51675); β-actin-forward 5′-GGCTGTGCTATCCCTGTACGCC-3′ and -reverse 5′-GGGCAGTGATCTCCTTCTGCAT-3′ (accession No. X00351); GAPDH-forward 5′-GGTCTCCTCTGACTTCAACAGCG-3′ and -reverse 5′-GGTACTTTATTGATGGTACATGAC-3′ (accession No. M33197). PCR, RT–PCR and probe preparation were carried out as described previously (Wary *et al*., 1993).

Biochemical methods

For western blot analysis, cells were washed with cold PBS, and solubilized in modified RIPA buffer (50 mM HEPES pH 7.5, 1.0% Triton X-100, 0.1% SDS, 0.25% deoxycholate, 150 mM sodium chloride, 1 mM EDTA, 25 mM sodium fluoride, 1 mM sodium pyrophosphate, 2 mM sodium orthovanadate and appropriate concentrations of various protease inhibitors). For cell surface biotinylation, HEK293 cells (5×10^6) were transfected with either pEGFP-C3, pEGFP-N3, pEGFP-C3-VCIP or pEGFP-N3-VCIP using Superfect-Liposome (Qiagen). Biotinylation of cell surface proteins was carried out according to published procedures (Gottardi *et al*., 1995). Immunoprecipitation, immunoblotting and immunodetection protocols were all performed as described previously (Mainiero *et al*., 1995, 1997; Wary *et al*., 1996, 1998, 1999a,b).

[^{35}S]Cys/Met labeling of HdMVEC and affinity chromatography

HdMVECs (3×10^7) were deprived of growth factors in Cys/Met-free DMEM for 8 h. Cells were incubated with 3 mCi of [^{35}S]Cys/Met (specific activity 1170.0 Ci/mmol) for 3 h at 37°C in Cys/Met-free media in the presence of 1× ITS. After 3 h, cells were rinsed twice with complete media and allowed to recover in complete media for 1 h at 37°C. Cells were then washed and solubilized in 4 ml of complete cell extraction buffer (CCEB: 50 mM HEPES pH 7.4, 150 mM sodium

chloride, 1% Triton X-100, 0.1% β-octylglucoside, 1 mM $MgCl_2$, 2 mM $CaCl_2$, with freshly added 2 mM PMSF, 10 μg/ml aprotinin, 5 μg/ml leupeptin and 10 μg/ml pepstatin-A as protease inhibitors). Cell extracts were clarified, pre-adsorbed once with 1.5 ml of packed Sepharose beads coupled to GST-fusion proteins (2 mg/ml) and once with 1.0 ml (packed) anti-mouse IgG agarose for 2 h each at 4°C. Pre-adsorbed lysates were divided into two tubes, and 7 μg of GST–VCIP-RGD fusion protein was added to each sample. One of the tubes included the GRGDSP synthetic soluble peptide (25 μM). GST-pull down was carried out at 4°C for 8 h, complexes washed once with CCEB, three times with GST-fusion protein wash buffer (50 mM HEPES pH 7.4, 150 mM sodium fluoride, 5% glycerol, 0.5% NP-40, 1 mM $CaCl_2$ and 1 mM $MgCl_2$) and one final wash with 1× TBS pH 7.4. The contents of the other tube were resuspended in 0.5 ml of dissociation buffer (10 mM Tris pH 7.4, 0.75% SDS, 1% Triton X-100 and 250 mM NaCl), boiled for 10 min, centrifuged immediately and the beads were discarded. The supernatant was diluted with 4 ml of dilution buffer: 10 mM Tris pH 7.4, 100 mM NaCl, 1.0% Triton X-100, 2 mM $CaCl_2$ and 2 mM $MgCl_2$. This was equally divided into tubes containing 5 μg of either anti-mouse IgG, anti-$\alpha_v\beta_3$ (LM609) or anti-$\alpha_5\beta_1$ (P1D6) integrin monoclonal antibodies. Immunoprecipitates were washed three times with cold CCEB and once with cold 1× TBS pH 7.4. Samples were boiled in non-reducing sample buffer and resolved by SDS–PAGE gradient gel. Gel was incubated in 1 M sodium salicylic acid, fixed, dried and exposed to X-ray film for 18 h at room temperature.

Recombinant cDNA constructs and transfection of cells

In order to generate GFP–VCIP constructs, PCR primers containing *Bam*HI (5′) and *Hin*dIII (3′) restriction sites were designed. The GFP gene was inserted in-frame with the VCIP gene (on either the N-terminus or C-terminus) into the mammalian expression plasmids pEGFP-N3 or pEGFP-C3, thereby, encoding pEGFP-VCIP-N3 or pEGFP-VCIP-C3 fusion proteins (Figure 3A–D). For retroviral constructs, the human VCIP cDNA was subcloned into pLNCX2 (Clontech) immediately downstream of the human CMV immediate early promoter. Two-step PCR was used to insert three copies of an HA-tag (YPYDVPDYA) at the N-terminus of the VCIP cDNA and to mutate the wild-type RGD sequence in one of the proteins to RGE (Figure 3E–G). The two-step PCR method has been described previously (Wary *et al*., 1996). Amphopack-293 packaging cells (Clontech) were transfected with pLNCX2 (V), pLNCX2-VCIP-RGD (WT) and pLNCX2-VCIP-RGE (MT) using Superfect lipososme (Qiagen). Supernatants collected from stably transfected packaging cell lines were incubated with 60% confluent HEK293 cells in presence of polybrene (8 μg/ml). For GST-fusion proteins, two-step PCR was used to mutate the wild-type RGD sequence in one of the proteins to RGE (Figure 3H–J). Fragments were subcloned into the *Bam*HI and *Hin*dIII restriction sites of the pGstag vector (Ron and Dressler, 1992), and constructs were confirmed by DNA sequencing. The GST–VCIP-RGD and GST–VCIP-RGE recombinant proteins were expressed in *Escherichia coli* (BL21) cells and affinity purified using Sepharose–glutathione beads. GST-fusion proteins were dialyzed against 20 mM Tris–HCl pH 7.5, containing 175 mM sodium chloride and 20 mM potassium chloride.

Cell aggregation assay

To monitor aggregation, cells were labeled with optimal non-toxic concentrations of fluorescent dyes. This assay was performed essentially according to the protocol described by Niessen and Gumbiner (2002), with minor modifications. Briefly, pLNCX2-VCIP-RGD-HEK (WT) and pLNCX2-VCIP-RGD-HEK (MT) cells were detached from dishes with 0.025% trypsin and 2 mM EDTA, washed with PBS and passed through a cell strainer. Cells were collected and resuspended in HCMF buffer (20 mM HEPES pH 7.4, 137.5 mM NaCl, 5.0 mM KCl, 0.35 mM $Na_2HPO_4{\cdot}7\,H_2O$, 4.5 mM glucose and 10 mM $CaCl_2$) supplemented with 5 mM Ca^{2+}, 1 mM Mg^{2+}, 10 μg/ml of 3,3-dioctadecycloxacarbocyanine perchlorate (DiO) and 2.5 μg/ml of 1,1′-dioctadecyl-3,3,3,′3′-tetramethylindocarbocyanine perchlorate (Dil) (Molecular Probes) at 37°C for 8 min. Red and green cells (0.5×10^6 of each) were allowed to aggregate in 500 μl of HCMF in the presence of 50 U/ml DNase I containing either Ca/Mg, peptides or EDTA, or anti-VCIP-RGD or control antibodies in siliconized cylindrical glass vials by rotating at 90 r.p.m. at 37°C for 0, 6 or 12 h. The inhibitory effects of EDTA, peptides and antibodies on cell aggregation were determined at the end of 12 h. A graticule was placed inside a 10× eyepiece to aid enumeration of cell aggregates. A minimum of seven random fields were used for each point. Experiments were performed at least three times with each point analyzed in triplicate. Only productive cell aggregates (yellow) were counted. Unproductive WT (red) cell aggregates were ignored. Numbers were expressed as the percentage of total aggregates counted.

Cell proliferation, apoptosis and immunofluorescence microscopy

The methods used to measure proliferation and score apoptosis have been described previously (Wary *et al*., 1996). Briefly, cells were deprived of growth factors for 24 h. The next day, cells were replenished with defined media containing 10 μM BrdU and returned to the 37°C incubator for 16–18 h. Cells were then fixed and permeabilized by acid treatment, immunostained with an anti-BrdU monoclonal antibody and an alkaline phosphatase-conjugated secondary antibody, then counterstained with hematoxylin. The BrdU-positive cells were scored from three independent experiments, performed in triplicate. A minimum of five random fields was selected on each coverslip at 100× magnification. The percentage of BrdU incorporation was determined as a measure of the number of cells entering the S phase of the cell cycle. For the apoptosis assay, cells were deprived of growth factors for 24 h, then incubated in defined medium for 28 h. Attached and unattached cells were combined, fixed with cold 20 mM glycine–HCl pH 2.0 and stained in suspension with Hoechst 33258 dye (0.5 μg/ml). Cells were examined under a Zeiss Axiovert-125 fluoroscope. The presence of more than two visible nuclear fragments was considered as a single apoptotic event. Apoptotic events were counted from at least five random microscopic fields.

Solid phase ELISA and adhesion blocking assay

Solid phase ligand binding assays were performed according to a previously published procedure (Orlando and Cheresh, 1991). Briefly, soluble $\alpha_2\beta_1$, $\alpha_5\beta_1$, $\alpha_v\beta_3$ and $\alpha_v\beta_5$ integrins (1 μg/ml in a solution containing 20 mM Tris pH 7.4, 150 mM NaCl, 1 mM $CaCl_2$, 1 mM $MgCl_2$ and 1 mM $MnCl_2$) were immobilized onto 96-well microtiter plates at 4°C. Wells were washed and blocked with 0.5% BSA. After washing, the GST, GST–VCIP-RGD and GST–VCIP-RGE ligands were added (50–350 ng per well in a solution of TBS pH 7.4) and incubated at 37°C for 1 h. After washing, the wells were incubated with the anti-GST (sc-138, Santa Cruz) monoclonal antibody for 1 h, followed by washing and incubation with a horseradish peroxidase (HRP)-conjugated mouse secondary antibody. Plates were then washed again and the ABTS substrate (Bio-Rad) was added. All washing steps were carried out using PBS. Absorbances were read at 405 nm, and non-specific binding values were adjusted against BSA.

For adhesion blocking assays, ECs were detached, washed with PBS and resuspended in M199 media containing 1 mM $CaCl_2$ and 1 mM $MgCl_2$ in the absence of serum or growth factors. ECs (2×10^5 cells) were replated onto 24-well tissue culture plates coated with 1, 5 and 10 nM affinity purified GST–VCIP-RGE and GST–VCIP-RGD fusion proteins. Cells were allowed to reattach for 45 min, then washed, fixed with 4% paraformaldehyde, stained with 0.5% crystal violet for 5 min and then washed extensively with water. Absorbances were measured at 540 nm. To monitor the effects of anti-integrin antibodies, dishes were coated with 10 nM GST–VCIP-RGD, immobilized with 1.0% glutaraldehyde in PBS and washed several times with PBS prior to use. ECs (5×10^5 cells in 300 μl PBS) were pre-incubated at 4°C with 1, 5 or 10 μg/ml of anti-$\alpha_5\beta_1$ (P1D6, Invitrogen), anti-$\alpha_v\beta_3$ (LM609, Chemicon), anti-$\alpha_2\beta_1$ (MAB 1998, Chemicon) and anti-$\alpha_3\beta_1$ (P1B5, Invitrogen) antibodies for 30 min. Cells were then washed with PBS containing Ca^{2+} and Mg^{2+}, and replated onto coated dishes. After 45 min, cells were washed, fixed and stained with 0.05% crystal violet for 10 min. After extensive washing, absorbances of eluted dyes were measured at 590 nm.

Immunostaining of tumor sections

Double immunostaining of paraffin-embedded tumor sections (4 μm) was performed following antigen retrieval. Specimens were subjected to microwave treatment (1000 W) in citrate buffer pH 6.0, four times for 5 min each. Peroxidase activity was then inhibited by the addition of 3% H_2O_2 in PBS for 20 min, followed by blocking with 3% BSA in PBS. Sections were then incubated with the affinity purified anti-VCIP-RGD antibody (20 μg/ml), followed by either anti-VEGF (30 μg/ml), vWF (50 μg/ml) or anti-$\alpha_v\beta_3$ integrin (30 μg/ml) antibodies. After incubation with primary antibodies, slides were washed with PBS. Incubation with Texas Red-conjugated anti-rabbit IgGs and with FITC-conjugated goat anti-mouse IgGs was used to detect VCIP (red), vWF (green) and $\alpha_v\beta_3$ (green) integrin, respectively.

Statistical analysis

Statistical significance was determined by performing the Student's *t*-test. All experiments were carried out at least three times.

Supplementary data

Supplementary data are available at *The EMBO Journal* Online.

Acknowledgements

We thank Drs Magnus Höök, Mingyao Liu and Filippo G.Giancotti for useful discussions. The technical assistance of Kimberly Bryant is gratefully acknowledged. This work was made possible by the new faculty start-up fund provided by the Institute of Biosciences and Technology (K.K.W.) and an award from American Heart Association (K.K.W.).

References

Abedi,H. and Zachary,I. (1995) Signalling mechanisms in the regulation of vascular cell migration. *Cardiovasc. Res.*, **30**, 544–556.

Assoian,R.K. and Marcantonio,E.E. (1996) The extracellular matrix as a cell cycle control element in atherosclerosis and restenosis. *J. Clin. Invest.*, **98**, 2436–2439.

Carmeliet,P. and Jain,R.K. (2000) Angiogenesis in cancer and other diseases. *Nature*, **407**, 249–257.

Carmeliet,P. *et al*. (1996) Abnormal blood vessel development and lethality in embryos lacking a single VEGF allele. *Nature*, **380**, 435–439.

Cines,D.B. *et al*. (1998) Endothelial cells in physiology and in the pathophysiology of vascular disorders. *Blood*, **91**, 3527–3561.

Cotta-Pereira,G., Sage,H., Bornstein,P., Ross,R. and Schwartz,S. (1980) Studies of morphologically atypical ('sprouting') cultures of bovine aortic endothelial cells. Growth characteristics and connective tissue protein synthesis. *J. Cell Physiol.*, **102**, 183–191.

Cross,M.J. and Claesson-Welsh,L. (2001) FGF and VEGF function in angiogenesis: signalling pathways, biological responses and therapeutic inhibition. *Trends Pharmacol. Sci.*, **22**, 201–207.

Darland,D.C. and D'Amore,P.A. (2001) Cell–cell interactions in vascular development. *Curr. Top. Dev. Biol.*, **52**, 107–149.

Dejana,E. (1997) Endothelial adherens junctions: implications in the control of vascular permeability and angiogenesis. *J. Clin. Invest.*, **100**, S7–S10.

Dufourcq,P., Louis,H., Moreau,C., Daret,D., Boisseau,M.R., Lamaziere,J.M. and Bonnet,J. (1998) Vitronectin expression and interaction with receptors in smooth muscle cells from human atheromatous plaque. *Arterioscler. Thromb. Vasc. Biol.*, **18**, 168–176.

Dvorak,H.F. (2000) VPF/VEGF and the angiogenic response. *Semin. Perinatol.*, **24**, 75–78.

Eliceiri,B.P. and Cheresh,D.A. (2001) Adhesion events in angiogenesis. *Curr. Opin. Cell Biol.*, **13**, 563–568.

Folkman,J. (2001) Angiogenesis-dependent diseases. *Semin. Oncol.*, **28**, 536–542.

Friesel,R.E. and Maciag,T. (1995) Molecular mechanisms of angiogenesis: fibroblast growth factor signal transduction. *FASEB J.*, **9**, 919–925.

Frisch,S.M. and Ruoslahti,E. (1997) Integrins and anoikis. *Curr. Opin. Cell Biol.*, **9**, 701–706.

Giancotti,F.G. and Ruoslahti,E. (1999) Integrin signaling. *Science*, **285**, 1028–1032.

Gottardi,C.J., Dunbar,L.A. and Caplan,M.J. (1995) Biotinylation and assessment of membrane polarity: caveats and methodological concerns. *Am. J. Physiol.*, **268**, F285–F295.

Hanahan,D. and Folkman,J. (1996) Patterns and emerging mechanisms of the angiogenic switch during tumorigenesis. *Cell*, **86**, 353–364.

Harlow,E. and Lane,D. (1988) *Antibodies: A Laboratory Manual*. Cold Spring Harbor Laboratory Press, Cold Spring Harbor, NY.

Hirschi,K.K. and D'Amore,P.A. (1997) Control of angiogenesis by the pericyte: molecular mechanisms and significance. *EXS*, **79**, 419–428.

Hoshiga,M., Alpers,C.E., Smith,L.L., Giachelli,C.M. and Schwartz,S.M. (1995) Alpha-v beta-3 integrin expression in normal and atherosclerotic artery. *Circ. Res.*, **77**, 1129–1135.

Humphries,M.J. (2002) Insights into integrin-ligand binding and activation from the first crystal structure. *Arthritis Res.*, **4**, S69–S78.

Hynes,R.O. (1987) Integrins: a family of cell surface receptors. *Cell*, **48**, 549–554.

Ishikawa,T., Kai,M., Wada,I. and Kanoh,H. (2000) Cell surface activities of the human type 2b phosphatidic acid phosphatase. *J. Biochem. (Tokyo)*, **127**, 645–651.

Jasinska,R. *et al*. (1999) Lipid phosphate phosphohydrolase-1 degrades exogenous glycerolipid and sphingolipid phosphate esters. *Biochem. J.*, **340**, 677–686.

Kai,M., Wada,I., Imai,S., Sakane,F. and Kanoh,H. (1997) Cloning and characterization of two human isozymes of Mg^{2+}-independent phosphatidic acid phosphatase. *J. Biol. Chem.*, **272**, 24572–24578.

Lampugnani,M.G. and Dejana,E. (1997) Interendothelial junctions: structure, signalling and functional roles. *Curr. Opin. Cell Biol.*, **9**, 674–682.

Luscinskas,F.W., Kansas,G.S., Ding,H., Pizcueta,P., Schleiffenbaum,B.E., Tedder,T.F. and Gimbrone,M.A.,Jr (1994) Monocyte rolling, arrest and spreading on IL-4-activated vascular endothelium under flow is mediated via sequential action of L-selectin, β_1-integrins, and β_2-integrins. *J. Cell Biol.*, **125**, 1417–1427.

Madri,J.A. and Williams,S.K. (1983) Capillary endothelial cell cultures: phenotypic modulation by matrix components. *J. Cell Biol.*, **97**, 153–165.

Mainiero,F., Pepe,A., Wary,K.K., Spinardi,L., Mohammadi,M., Schlessinger,J. and Giancotti,F.G. (1995) Signal transduction by the $\alpha_6\beta_4$ integrin: distinct β_4 subunit sites mediate recruitment of Shc/Grb2 and association with the cytoskeleton of hemidesmosomes. *EMBO J.*, **14**, 4470–4481.

Mainiero,F., Murgia,C., Wary,K.K., Curatola,A.M., Pepe,A., Blumemberg,M., Westwick,J.K., Der,C.J. and Giancotti,F.G. (1997) The coupling of $\alpha_6\beta_4$ integrin to Ras-MAP kinase pathways mediated by Shc controls keratinocyte proliferation. *EMBO J.*, **16**, 2365–2375.

Martin,K.H., Slack,J.K., Boerner,S.A., Martin,C.C. and Parsons,J.T. (2002) Integrin connections map: to infinity and beyond. *Science*, **296**, 1652–1653.

McEver,R.P. (2001) Adhesive interactions of leukocytes, platelets, and the vessel wall during hemostasis and inflammation. *Thromb. Haemost.*, **86**, 746–756.

Montesano,R. and Orci,L. (1985) Tumor-promoting phorbol esters induce angiogenesis *in vitro*. *Cell*, **42**, 469–477.

Montesano,R., Orci,L. and Vassalli,P. (1985) Human endothelial cell cultures: phenotypic modulation by leukocyte interleukins. *J. Cell Physiol.*, **122**, 424–434.

Muller,W.A. (2002) Leukocyte-endothelial cell interactions in the inflammatory response. *Lab. Invest.*, **82**, 521–533.

Niessen,C.M. and Gumbiner,B.M. (2002) Cadherin-mediated cell sorting not determined by binding or adhesion specificity. *J. Cell Biol.*, **156**, 389–399.

Orlando,R.A. and Cheresh,D.A. (1991) Arginine-glycine-aspartic acid binding leading to molecular stabilization between integrin $\alpha_v\beta_3$ and its ligand. *J. Biol. Chem.*, **266**, 19543–1955.

Pepper,M.S., Ferrara,N., Orci,L. and Montesano,R. (1992) Potent synergism between vascular endothelial growth factor and basic fibroblast growth factor in the induction of angiogenesis *in vitro*. *Biochem. Biophys. Res. Commun.*, **189**, 824–831.

Plow,E.F., Haas,T.A., Zhang,L., Loftus,J. and Smith,J.W. (2000) Ligand binding to integrins. *J. Biol. Chem.*, **275**, 21785–21788.

Pozzi,A., Wary,K.K., Giancotti,F.G. and Gardner,H.A. (1998) Integrin $\alpha_1\beta_1$ mediates a unique collagen-dependent proliferation pathway *in vivo*. *J. Cell Biol.*, **142**, 587–594.

Risau,W. and Flamme,I. (1995) Vasculogenesis. *Annu. Rev. Cell. Dev. Biol.*, **11**, 73–91.

Roberts,R., Sciorra,V.A. and Morris,A.J. (1998) Human type 2 phosphatidic acid phosphohydrolases. Substrate specificity of the type 2a, 2b, and 2c enzymes and cell surface activity of the 2a isoform. *J. Biol. Chem.*, **273**, 22059–22067.

Ron,D. and Dressler,H. (1992) pGSTag–a versatile bacterial expression plasmid for enzymatic labeling of recombinant proteins. *Biotechniques*, **13**, 866–869.

Ruoslahti,E. and Pierschbacher,M.D. (1987) New perspectives in cell adhesion: RGD and integrins. *Science*, **238**, 491–497.

Schlaepfer,D.D., Hanks,S.K., Hunter,T. and van der Geer,P. (1994) Integrin-mediated signal transduction linked to Ras pathway by GRB2 binding to focal adhesion kinase. *Nature*, **372**, 786–791.

Schwartz,M.A. and Ginsberg,M.H. (2002) Networks and crosstalk: integrin signalling spreads. *Nat. Cell Biol.*, **4**, E65–E68.

Shalaby,F., Rossant,J., Yamaguchi,T.P., Gertsenstein,M., Wu,X.F., Breitman,M.L. and Schuh,A.C. (1995) Failure of blood-island formation and vasculogenesis in Flk-1-deficient mice. *Nature*, **376**, 62–66.

Stukey,J. and Carman,G.M. (1997) Identification of a novel phosphatase sequence motif. *Protein Sci.*, **6**, 469–472.

Suri,C., Jones,P.F., Patan,S., Bartunkova,S., Maisonpierre,P.C., Davis,S., Sato,T.N. and Yancopoulos,G.D. (1996) Requisite role of

angiopoietin-1, a ligand for the TIE2 receptor, during embryonic angiogenesis. *Cell*, **87**, 1171–1180.

Tailor,A. and Granger,D.N. (2000) Role of adhesion molecules in vascular regulation and damage. *Curr. Hypertens. Rep.*, **2**, 78–83.

Thakker,G.D., Hajjar,D.P., Muller,W.A. and Rosengart,T.K. (1999) The role of phosphatidylinositol 3-kinase in vascular endothelial growth factor signaling. *J. Biol. Chem.*, **274**, 10002–10007.

Varner,J.A. and Cheresh,D.A. (1996) Integrins and cancer. *Curr. Opin. Cell Biol.*, **8**, 724–730.

Wang,H.U., Chen,Z.F. and Anderson,D.J. (1998) Molecular distinction and angiogenic interaction between embryonic arteries and veins revealed by ephrin-B2 and its receptor Eph-B4. *Cell*, **93**, 741–753.

Wary,K.K., Lou,Z., Buchberg,A.M., Siracusa,L.D., Druck,T., LaForgia,S. and Huebner,K. (1993) A homozygous deletion within the carbonic anhydrase-like domain of the Ptprg gene in murine L-cells. *Cancer Res.*, **53**, 1498–1502.

Wary,K.K., Mainiero,F., Isakoff,S.J., Marcantonio,E.E. and Giancotti,F.G. (1996) The adaptor protein Shc couples a class of integrins to the control of cell cycle progression. *Cell*, **87**, 733–743.

Wary,K.K, Mariotti,A., Zurzolo,C. and Giancotti,F.G. (1998) A requirement for caveolin-1 and associated kinase Fyn in integrin signaling and anchorage-dependent cell growth. *Cell*, **94**, 625–634.

Wary,K.K., Dans,M., Mariotti,A. and Giancotti,F.G. (1999a) Biochemical analysis of integrin-mediated Shc signaling. In Howlett,A. (ed.), *Methods in Molecular Biology*. Humana Press, Totowa, NJ, 35–49.

Wary,K.K., Mariotti,A., and Giancotti,F.G. (1999b) Specificity of integrin signaling. In Guan,J.L. (ed.), *Signaling through Cell Adhesion Molecules*. CRC Press, Boca Raton, FL, 101–114.

Yancopoulos,G.D., Klagsbrun,M. and Folkman,J. (1998) Vasculogenesis, angiogenesis, and growth factors: ephrins enter the fray at the border. *Cell*, **93**, 661–664.

Yancopoulos,G.D., Davis,S., Gale,N.W., Rudge,J.S., Wiegand,S.J. and Holash,J. (2000) Vascular-specific growth factors and blood vessel formation. *Nature*, **407**, 242–248.

Received September 29, 2002; revised January 20, 2003; accepted February 17, 2003